Biomedicine & Pharmacotherapy 142 (2021) 112006

Contents lists available at ScienceDirect

Biomedicine & Pharmacotherapy

journal homepage: www.elsevier.com/locate/biopha

Physalin pool from *Physalis angulata* L. leaves and physalin D inhibit P2X7 receptor function in vitro and acute lung injury in vivo

J.C.C. Arruda [a], N.C. Rocha [g], E.G. Santos [c], L.G.B. Ferreira [f], M.L. Bello [c], C. Penido [d,e], T.E.M. M. Costa [d,e], J.A.A. Santos [b], I.M. Ribeiro [d], T.C.B. Tomassini [d], R.X. Faria [b,g,*]

[a] University Center Foundation of the West Zone of Rio de Janeiro, Rio de Janeiro, Brazil
[b] Laboratory of Evaluation and Promotion of Environmental Health, Oswaldo Cruz Institute, FIOCRUZ, Rio de Janeiro, Brazil
[c] Laboratory of Pharmaceutical Planning and Computer Simulation, Faculty of Pharmacy, Federal University of Rio de Janeiro, Rio de Janeiro, Brazil
[d] Laboratory of Research in Chemistry of Natural Products (Farmanguinhos), Rio de Janeiro, Brazil
[e] Laboratory of Applied Pharmacology, Institute of Drug Technology (Farmanguinhos), Rio de Janeiro, Brazil
[f] Laboratory of Inflammation, Oswaldo Cruz Institute, FIOCRUZ, Rio de Janeiro, Brazil
[g] Postgraduate Program in Sciences and Biotechnology, Institute of Biology, Fluminense Federal University, Niterói, RJ, Brazil

ARTICLE INFO

Keywords:
Anti-inflammatory
Lung
Pre-clinical
Purinergic receptors
Pore formation
Natural products

ABSTRACT

P2X7 receptor promotes inflammatory response and neuropathic pain. New drugs capable of impairing inflammation and pain-reducing adverse effects extracted from plant extracts have been studied. *Physalis angulate* L. possesses traditional uses and exhibits antiparasitic, anti-inflammatory, antimicrobial, antinociceptive, antimalarial, antileishmanial, immunosuppressive, antiasthmatic. diuretic, and antitumor activities. The most representative phytochemical constituents identified with medicinal importance are the physalins and withanolides. However, the mechanism of anti-inflammatory action is scarce. Although some physalins and withanolides subtypes have anti-inflammatory activity, only four physalins subtypes (B, D, F, and G) have further studies. Therefore, we evaluated the crude ethanolic extract enriched with physalins B, D, F, and G from *P. angulata* leaves, a pool containing the physalins B, D, F, G, and the physalins individually, as P2X7 receptor antagonists. For this purpose, we evaluated ATP-induced dye uptake, macroscopic currents, and interleukin 1-β (IL-1β) in vitro. The crude extract and pool dose-dependently inhibited P2X7 receptor function. Thus, physalin B, D, F, and G individually evaluated for 5′-triphosphate (ATP)-induced dye uptake assay, whole-cell patch-clamp, and cytokine release showed distinct antagonist levels. Physalin D displayed higher potency and efficacy than physalin B, F, and G for all these parameters. In vivo mice model as ATP-induced paw edema was potently inhibited for physalin D, in contrast to physalin B, F, and G. ATP and lipopolysaccharide (LPS)-induced pleurisy in mice were reversed for physalin D treatment. Molecular modeling and computational simulation predicted the

Abbreviations: 2D, two dimension; A438079, 3-[[5-(2,3-Dichlorophenyl)-1H-tetrazol-1-yl]methyl]pyridine hydrochloride; A740003, N-(1-{[(cyanoimino)(5-quinolinylamino) methyl] amino}-2,2-dimethylpropyl)-2-(3,4-dimethoxyphenyl)acetamide; AEC I, type I alveolar cells; AGL, Agelasine; ALI, Acute Lung Injury; ANOVA, Analysis of variance; AR-C 118925XX, 5-[[5-(2,8-Dimethyl-5H-dibenzo[*a*,*d*]cyclohepten-5-yl)-3,4-dihydro-2-oxo-4-thioxo-1(2H)-pyrimidinyl]methyl]-N-2H-tetrazol-5-yl-2-furancarboxamide; ARDS, Acute respiratory distress syndrome; ATP, Adenosine 5′-triphosphate; BALF, Bronchoalveolar lavage fluid; BBG, Brilliant Blue G; BzATP, 2′(3′)-O-(4-Benzoylbenzoyl)adenosine 5′-triphosphate; CO_2,, Carbon monoxide; CFA, Complete Freund's adjuvant; CD, Cluster of differentiation; DCFH2-DA, 2′,7′-Dichlorofluorescin Diacetate; DNA, DeoxyriboNucleic acid; DMSO, Dimethyl sulphoxide; DMEM, Dulbecco's modified Eagle's medium; FACS, Fluorescence-activated cell sorting; FBS, Fetal bovine sérum; GA, garcinolic acid; GR, glucocorticoid receptor; HCS, High Content Screening; HEPES, 4-(2-hydroxyethyl)-1-piperazineethanesulfonic acid; HEK-293, Human Embryonic Kidney 293; IFN-γ, interferon-γ; IL-1β, interleukin 1-β; IL-6, interleukin-6; IL-18, interleukin-18; KN-62, 4-[(2S)-2-[(5-isoquinolinylsulfonyl)methylamino]-3-oxo-3-(4-phenyl-1-piperazinyl)propyl] phenyl isoquinolinesulfonic acid ester; KO, knockout; LDH, Lactate dehydrogenase; LPS, lipopolysaccharide; MVD, Molegro Virtual Docker; MPO, myeloperoxidase; RU486, Mifepristone; NAD, Nicotinamide; NLRP3, Nucleotide oligomerization domain-like receptor protein 3; NO, nitric oxide; NOD, Nucleotide oligomerization domain; NPT, amount of substance (N), pressure, and temperature (T); NVT, amount of substance (N), volume (V) and temperature (T); PBS, Phosphate-buffered saline; PE/Cy5, Streptavidin-Phycoerythrin/Cy5; PI, Propidium iodide; PME, Particle Mesh Ewald; ROS, reactive oxygen species; RMS, Root Mean Square; RMSD, Root Mean Square Deviation; RPMI, Roswell Park Memorial Institute 1640; SAP, severe acute pancreatitis; STDs, Sexually transmitted diseases; TLR4, Toll-like receptor 4; TNF-α, Tumor Necrosis Factor-α; STAT, Signal transducer and activator of transcription; YFP, Yellow fluorescent protein; YFP-GR fusion, yellow fluorescent protein fused with glucocorticoid receptor.

* Correspondence to: Fundação Oswaldo Cruz, Instituto Oswaldo Cruz, Laboratório de Avaliação e Promoção da Saúde Ambiental, Avenida Brasil 4365, Pavilhão Lauro Travassos, sl 01, Manguinhos, CEP 21040-900 Rio de Janeiro, RJ, Brazil.
E-mail address: salvador@ioc.fiocruz.br (R.X. Faria).

https://doi.org/10.1016/j.biopha.2021.112006
Received 26 February 2021; Received in revised form 14 July 2021; Accepted 1 August 2021
Available online 12 August 2021

intermolecular interactions between the P2X7 receptor and physalin derivatives. *In silico* results indicated physalin D and F as a potent allosteric P2X7 receptor antagonist. These data confirm physalin D as a promisor source for developing a new P2X7 receptor antagonist with anti-inflammatory action.

1. Introduction

The medicinal plant extracts increased scientific interest in pharmacological properties and chemical composition [1–4]. The plant kingdom is an inexhaustible fount of molecules susceptible to pharmacopeia [5]. Several plants used in folk medicine focus on scientific research for the commercialization and treatment of diseases.

The Solanaceae family has about 2500 species divided into 100 genera into several global regions. In South America, Brazil, this family possesses 31 genders and about 500 native species. This botanical family exhibit species diary used in food habits, such as potato (Solanum sp), tomato (Solanum sp), and tobacco (*Nicotiana tabacum* sp) [6].

Physalis genus has a source of substances derived from ergostane, mainly polioxigenates vitaesterols, epoxides [7], and enones [8], acting as chemical constituents responsible for the activities: [9], antimicrobial [10,11], and anticancer [12,13]. Additionally, there are a description of glycosylated flavonoids (kaempferol, quercetin, and rutin – with one, two, or three units of sugar) [14,15], steroids (β-sitosterol, stigmasterol, Campesterol, 24-methylene cholesterol, among others), straight-chain fatty acids (C6 to C24), hydroxylated, epoxidized carotenoids and ascorbic acid and alkaloids [16,17].

Physalis angulata L. is a natural herb distributed in many countries located in tropical and subtropical regions [18]. This plant is popularly known as Joah [18] and is used in folk medicine to treat various diseases [19]. Pre-clinical assays demonstrated anti-tumor, trypanocidal, anti-inflammatory [20], leishmanicidal [21], antimalarial, antidiabetic, anti-hepatitis, antiasthmatic [22], antibacterial [22,23], and activity against some sexually transmitted diseases (STDs) [24]. This plant modulates the immune system, specifically regulating the inflammation and pro-inflammatory cytokine production in mice [20,25].

Adenosine triphosphate (ATP) is a critical inflammatory response mediator. When present in the extracellular medium, the ATP activates P2 receptors, and particularly the P2X7 receptor. This P2X receptor subtype modulates the inflammatory responses, pain [26], and some types of cancer [27]. Concerning inflammatory response, the P2X7 receptor regulates the production of the pro-inflammatory cytokines, including interleukin (IL)-1, tumor necrosis factor (TNF)-α, and interleukin-6 (IL-6) [28,29]. Additionally, P2X7R activation in high glucose (HG) conditions lead to pro-inflammatory markers over-expression. This state promotes retinal blood barrier (BRB) breakdown, which is a characteristic of diabetic retinopathy (DR) [30,31]. Eyes of glaucoma animal models and patients contain high ATP concentration. The combination of elevated ATP levels activating the P2X7R, ischemia, or increased intraocular pressure (IOP) stimulates retinal ganglion cell (RGC) dysfunction and death and cytokine production [32–36]. Therefore, the expression on immune and microglial cells associated with the active participation of inflammatory factors secretion implicate the P2X7 receptor modulation in pathologic inflammation, chronic inflammatory pain in vitro [37,38], and clinical studies [39,40].

Based on the initial findings, the P2X7 receptor antagonists actuate as anti-inflammatory agents. Previously, natural products promoted inhibitory action against P2X7 receptor activity [41–43], and *P. angulata* inhibited the anti-inflammatory and immunomodulatory activities acting on cyclooxygenase-dependent and independent pathways [44]. Therefore, we investigated the P2X7 receptor function in the *P. angulata* crude extract and their isolated substances.

2. Material and methods

2.1. Plant

2.1.1. Extract and fractions preparation

Extracts, fractions, physalin pools, and isolated physalins were prepared for the Chemistry Laboratory of Natural Products, PN2 of Farmanguinhos.

P. angulata collection occurred in October 1995 in Belém, State of Pará, Brazil. Dr. Lúcia d'A Freire Carvalho identified the samples at Jardim Botânico, Rio de Janeiro, and was authenticated and stored at the Federal University of Rio de Janeiro herbarium, Botany Department, under the reference number RFA23907/8. The whole plant was dried at room temperature, ground, and measured with ethanol following a general procedure. Mabry modified technique was used in the extracts to prepare physalins pool. As a result, it is possible to get pure physalins containing Seco-ergostanes having 28 carbon atoms, a ketone at C15, two lactones (furan and pyran type) attached at C18 and C20 positions, respectively [45,46].

The physalins purification was described elsewhere and performed on a silica gel column and eluted by a stepwise gradient with a solvent mixture with progressively increasing polarity. The percent purity of physalins was realized by HPLC and was greater than 97% (47).

2.1.2. Identification of physalin D

Analysis HPLC was performed in triplicate using a Hibar Licchospher 100–18 column (250 mm × 4.0 mm; 5 μm particle size) on LC 20ADXR system consisted of an autosampler and SPD-M20A diode array detector. The gradient mobile programming was carried with acetonitrile and water acidified with TFA (0.05% v/v) at a flow rate of 1 mL/min^{-1} in methanol. The retention times and diode array spectra (225 and 310 nm) were used to identify the physalin D. Quantitation of physalin D determination was realized by a standard external method based on peak areas. The physalin D structure was detected by Electrospray Ionization Mass Spectrometry (ESI-MS) on a fourfold time-of-flight (Q-TOF) operated in positive ion mode [47].

The melting point was measured using digital equipment (model MQAPF-302) with a heating rate of 5 °C/min.

The Fourier Transform Infrared (FTIR) spectrum was recorded on a Thermo Scientific Nicolet 6700 FTIR spectrometer, using the Attenuated Total Reflectance (ATR) accessory with Germanium crystal and Deuterated Triglycine Sulfate (DTGS KBr) standard detector. Spectral data were collected from 4000 to 525 cm^{-1}, with 32 scans and 4 cm^{-1} resolutions.

1H and 13C nuclear magnetic resonance (NMR) spectra of physalin D were recorded on a spectrometer, model Avance 400 (Bruker, Bremen, Germany), 9.4 T, operating at the Larmor frequency at 400 MHz for 1H and 100 MHz for 13C. The spectra were acquired in DMSO-d6 at 22 ± 0.1 °C using pulses lengths of 11.5 μs for 1H and 10.0 μs for 13C and a 5 mm switchable probe. One hundred twenty-eight scans acquired 1H NMR spectra with a relaxation delay of 1.0 s, 64 K data points, 8012.8 Hz spectral width using a digital resolution of 0.30 Hz. The 13C spectra were acquired by 2048 scans with 24,038.5 Hz spectral width using a digital resolution of 1 Hz and 64 K data points. The chemical shifts (δ) were reported in ppm, using tetramethylsilane (TMS) as the reference and internal standard.

2.1.3. Extract, pool, and isolate physalins treatment

For in vitro assays, the extract, fraction, pool of physalins, and isolated physalins were dissolved into 10 mL of dimethyl sulphoxide

(DMSO) and diluted to 1000 mL with distilled water. Solutions were obtained in the following concentrations: 0.1 ng/mL to 500 mg/mL. The pool and isolated physalin doses tested in mice ranged from 0.1 ng/kg to 100 μg/kg.

2.2. In vitro assay

2.2.1. Mouse peritoneal macrophages

Peritoneal macrophages harvested from Swiss mice (male, 20–30 g) were isolated, centrifuged, re-suspended, and cultured, as described previously [48,49]. Our protocols follow the Ethical Principles in Animal Experimentation assumed by the Brazilian College of Animal Experimentation and accepted by the FIOCRUZ Research Ethics Committee (number L039-2016).

2.2.2. Human embryonic kidney 293 (HEK-293) cells transfected with human P2X7 receptor

HEK-293 cells [293T (ATCC® CRL-3216™), sixth passage] expressing human P2X7R were cultivated in Dulbecco's modified Eagle's medium (DMEM; Sigma-Aldrich. CA, USA) complemented with 10% fetal bovine serum (FBS; Prolab, Br), 50 mg/mL streptomycin, 50 U/mL penicillin in a humidified 5% CO_2 atmosphere at 37 °C [50]. The cells were plated at 37 °C in a quantity of 5×10^5 cells and humidified in a 5% CO_2 atmosphere for 24 h.

2.2.3. Human P2X7 receptor transfection

HEK293 cells were transfected for the present study to express the plasmid encoding the wild-type human P2X7 receptor sequence or with an empty vector. The hP2X7 plasmid (Qiagen, CH), a *Not*I-*Not*I insert of the human wild-type P2X7 coding sequence (GenBank accession number Y09561) within a pcDNA3 expression vector (Invitrogen). Briefly, cells (2×10^6) were transfected with plasmids (20–40 μg) encoding the human P2X7 receptor, or with an empty vector, by calcium phosphate precipitation, cloned and kept under selection presence of 0.2 mg/mL geneticin. RT-PCR and stimulation checked P2X7 receptor expression by the transfectants with benzoyl-ATP (BzATP) in the Ca^{2+} mobilization assay (Supplemental Fig. 1). HEK293 cells were cultured in DMEM-F12 (Sigma-Aldrich, Milan, Italy) supplemented with 10% fetal calf serum, 100 U/mL penicillin, and 100 μg/mL streptomycin (all from Celbio EuroClone, Milan, Italy).

2.2.4. RT-PCR

RNA extraction and qRT-PCR. HEK-293 cells expressing the human P2X7 receptor or not had their RNA extracted by Trizol reagent (Invitrogen), according to the manufacturer's instructions. The RNA yield and purity were evaluated using the NanoDrop ND-1000 (Thermo Scientific) instrument. First, the integrity was analyzed by a 1.2% agarose gel, using 200 ng of SBYR Green-II (Life Technologies) stained RNA. The RNA bands were visualized using a transilluminator system (L-Pix Touch, Loccus Biotecnologia). Then, 500 ng of RNA was reversed and transcribed according to SuperScript III (Invitrogen) of the manufacturer's protocol. The cDNA obtained was diluted (1:10), and 5 μL was used for PCR reaction. Briefly, the reaction was performed with 1X SYBR Green PCR Master Mix (Applied Biosystems), and 0.5 μM of primers at the final volume of 20 μL and was run on a StepOne Plus thermocycler (Applied Biosystems). The expression of P2X7 genes was normalized by reference endogenous control gene glyceraldehyde 3-phosphate dehydrogenase (GAPDH) expression values (Ct). Results are shown as gene relative expression (ΔCt). The real-time primer sequences used in this study was performed in a total volume of 20 μL, which included cDNA, each forward and reverse primer (Forward hP2X7R: 5′-AGATCGTGGAGAATGGAGTG-3′; Reverse hP2X7R: 5′-TCCTCGTGGTGTAGTTGTGG-3′; Forward hGAPDH: 5′-CGACCACTTTGTCAAGCTCA; Reverse hGAPDH: 5′-AGGGGTCTACATGGCAACTG-3′), and PCR master mix (Thermo Fisher Scientific).

2.2.5. Lactate dehydrogenase (LDH) release assay

LDH release was measured after treatment with 100 μg/mL–100 ng/mL crude ethanolic extract, 1 mg/mL–1 ng/mL pool of physalins, and isolated physalins. A quantity of 2×10^5 peritoneal macrophages cells per well was treated for 1, 3, 6, 24, 48, and 72 h. According to the manufacturer protocol, the supernatant collected from the treatments of the 96-well plate is used for the detection of the enzyme LDH (Doles, RJ, Brazil). After the centrifugation at 1500 rpm for 10 min, the supernatant (10 μL) was placed on a second plate. We left the plate in the greenhouse for 10 min. Next, the solution containing substrate (80 μL) + ferric alum (10 μL) was left in the oven for 5 min in a 35 mm Petri dish. This solution was added to the supernatant (10 μL) and left in the oven for 5 min (37 °C). Next, Nicotinamide (NAD; 5 μL) was added to each well for 5 min in the dark. Posteriorly, a stabilizer solution (50 μL of 1 N hydrochloric acid – HCl) was added. The white solution contains only the medium involved in the reaction. The sample was analyzed in a plate reading ($\lambda = 510$ nm) within 30 min afterward.

2.2.6. Dye uptake assay using flow cytometer technique

Fluorescent dye uptake assays performed with peritoneal macrophages, J774 cells, and HEK 293-transfected with P2X7 receptors were realized in a flow cytometer. The quantity of 2.6×10^5 cells per tube were incubated with the P2X7 receptor antagonists (500 nM and 750 nM BBG, 1 μM N-(1-{[(cyanoimino)(5-quinolinylamino) methyl] amino}-2,2-dimethyl propyl)-2-(3,4-dimethoxy phenyl)acetamide-A740003) and crude ethanolic extract (100 ng/mL–100 ug/mL), pool of physalins, and isolated physalins (1 ng/mL–1 ug/mL) for 10 min before 5 mM ATP addition for 20 min at 37 °C. In the last 5 min of ATP incubation, the deoxyribonucleic acid (DNA) intercalator propidium iodide (PI, 0.05 mg/mL in phosphate-buffered saline – PBS) was added. Summit software (Beckman Coulter, CA, EUA) was used to acquire and analyze the data. Triton-X 100 (0.5%) was used as a positive control, and all treatments were read in the Fluorescence-activated cell sorting (FACS) Calibur. PI was excited with a 488 nm laser, and the fluorescence emission was detected in a 620 nm filter.

2.2.7. Fluorescence microscopy (HCS – high content screening)

Peritoneal macrophages were cultivated for 48 h in a black plate with a light background (1×10^5 cells per mL, Grenier, USA) in a carbon monoxide (CO_2) oven at 37 °C. The culture medium was changed, and we treated these cells with P2X7 receptor antagonists or physalin extract and derivatives (10 min), followed by adding five mM ATP (15 min). In the final 5 min of ATP treatment, we added one μM PI (5 min) and observed the result in an HCS digital microscope (Molecular Devices, Sunnyvale, CA, USA). The photos were taken at three sites at each well, in the bright field and fluorescence. We used a 20× objective, a total final interval of 5 min, and a Streptavidin-Phycoerythrin/Cy5 (PE-Cy5) filter for PI reading performed by a laser scan. All microscopy data was analyzed by the CellProfiler (NIH, Cambridge, MA) and expressed in an average calculation of 50 cells per well.

Negative Control (Cells + PI); Positive Control (PI + Triton cells); 5 mM ATP; BBG 500 nM and 750 nM; A-740003 1 μM; physalins B, D, F, and G at concentrations of 10 ng/mL, 100 ng/mL and 1 μg/mL.

2.2.8. Electrophysiological measurements

Whole-cell configuration was performed as previously described [51]. Pipette serial resistance was 5–11 MΩ for all experiments in standard saline (bath and pipette solutions), and no compensation was applied for currents less than 1500 pA. Above this level, the ionic currents were compensated by 90%. Mice peritoneal macrophages (mean ± s.d., 23.06 ± 7.68 pF; n = 34) cell capacitance was measured by applying a −20 mV hyperpolarizing pulse from a holding potential of +20 mV; capacitive transient was integrated and divided by the magnitude of the voltage step (20 mV). Currents were filtered with a corner frequency of 5 kHz (8-pole Bessel filter), digitized at 20–50 kHz using a BNC- 2110 interface (National Instruments, TX, USA), and

acquired on a personal computer by using Axoscope software and pCLAMP 9.0 (Axon Instruments, CA, USA). Recordings were then filtered using a low-pass digital filter with a cutoff frequency of 500 Hz in the software (WinEDR V2.6.6.; University of Strathclyde, GL, UK). The bath solution (in mM) consisted of the following: 150 NaCl, 5 KCl, 1 $MgCl_2$, 1 $CaCl_2$, and 10 (4-(2-hydroxyethyl)-1-piperazineethanesulfonic acid) (HEPES) (pH, 7.4); and the pipette solution (in mM) consisted of the following: 150 KCl, 5 NaCl, 1 $MgCl_2$, 10 HEPES, and 0.1 EGTA (pH, 7.4). Patch-clamp experiments were realized under continuous perfusion (RC-24 chamber, Warner Instrument Corp., CT, USA). All drugs were dissolved in the saline solution immediately before use. Ion currents were studied by ATP pulse application (from 1 to 30 s).

2.2.9. IL-1β enzyme-linked immunosorbent assay

P2X7 receptor-mediated IL-1β release obtained from differentiated THP-1 cells (Laboratory of Applied Pharmacology, Institute of Drug Technology (Farmanguinhos), RJ, Brazil, sixth passage) stimulated with Escherichia coli lipopolysaccharide (LPS, serotype 0127: B8) before ATP addition. These cells plated at 2 × 105 cells/well in 96-well culture plates maintained in Roswell Park Memorial Institute 1640 (RPMI) containing 10% fetal bovine serum (FBS), penicillin (100 U/mL), and streptomycin (100 mg/mL) in a humidified 5% CO_2 atmosphere at 37 °C. Peritoneal macrophages from mice were treated with ten ng/mL of interferon-γ (IFN-γ) for 24 h. These cells were primate with 25 ng/mL LPS for 4 h. The second stimulus with ATP (5 mM) occurred in the last 30 min of the LPS incubation. P2X7 receptor antagonists (BBG and A740003) and physalins were added 30 min before the ATP stimulus. The supernatants were collected, centrifuged (1000 rpm for 5 min at 4 °C), and stored at −70 °C after LPS incubation. IL-1β was quantified using a standard kit (Bioscience, San Diego, CA, USA).

2.2.10. Statistical analysis

Statistical comparisons were expressed as mean ± SD (standard deviation), as indicated in the text. The statistical significance of divergences between means was examined by one-way analysis of variance (ANOVA), followed by Tukey's test. A bicaudal $p < 0.05$ was considered significant.

2.3. In vivo assay

2.3.1. Experimental mice

Swiss Webster male mice of 4–5 weeks from the Institute of Science and Technology in Biomodels/Fiocruz were used. In vivo protocols followed the Ethical Principles in Animal Experimentation adopted by the Brazilian College of Animal Experimentation and assumed by the FIOCRUZ Research Ethics Committee (number LW-5814 and LW-35/16).

2.3.2. ATP induced paw edema

ATP (10 mg/paw)-induced paw edema in mice was pretreated for 60 min with the sodium diclofenac (10 mg/kg), BBG (0.001–100 mg/kg), physalin pool or physalin B, D, F, and G (0.001–100 mg/kg). The antagonists were intraperitoneally administered before the intrathecal administration of ATP for 30 min. The edema formation was quantified for a mice plethysmometer (UGO Basil, Italy) before ATP injection compared with saline injection in the contralateral paw edema.

2.3.3. ATP and LPS-induced pleurisy

Male Swiss mice treated with intrathoracic (i.t.) injection of 0.1 mL of LPS (250 ng/cavity, from *E. coli* serotype 0127: B8), ATP (50 mg/cavity) or sterile saline (0.9%) (Control group) using an adapted needle (13 × 0.45 mm) carefully inserted at a depth of 1 mm into the right side of the thoracic cavity of mice. After the stimulus with ATP (50 mg/cavity) or LPS (250 ng/cavity) for 24 h, animals were euthanized with thiopental (150 mg/kg) for ATP and 10% Ketamine Hydrochloride and 2% Xylazine Hydrochloride for LPS assays, the thoracic cavity was opened and washed with 1 mL of heparinized saline (10 UI mL^{-1}). In addition, dexamethasone, BBG, physalin pool, physalin D, and Mifepristone (RU486) were orally administered. Pleural wash aliquots diluted in Turk solution (2% acetic acid) were counted in Neubauer chambers for obtaining the total leukocyte number. Differential leukocyte analyses were made using stained cytospins (Cytospin 3, Shandon Inc., Pittsburgh, PA) by the May-Grünwald-Giemsa method. Counts are described as numbers of cells per cavity.

2.3.4. Statistical analysis

Statistical comparisons were expressed as mean ± SD (standard deviation), as indicated in the text. The statistical significance of divergences between means was examined by one-way analysis of variance (ANOVA), followed by Tukey's test. A bicaudal $p < 0.05$ was considered significant.

2.4. Molecular modeling and computational simulation

2.4.1. Molecular modeling of ligands

Physalin derivatives were built using the program Avogadro [52]. Geometry optimizations were performed using the force field MMFF94 [53]. A followed geometry optimization was submitted to the semi-empirical method PM6 using the program MOPAC2016 [54,55].

2.4.2. Comparative modeling and lipid membrane model

The three-dimensional molecular model of the mouse P2X7 receptor ion channel was prepared using the program SWISS-MODEL [56]. The primary sequence with code entry Q9Z1M0 was obtained from the UniProtKB database [57]. A molecular structure template (code PDB: 5U1L) was obtained in the Protein Data Base [58]. The programs ProsA and PROCHECK were used to check the quality of the final model of mouse P2X7 receptor (Supplemental Figs. 2 and 3) [59,60].

The program CHARMM-GUI Membrane Builder was used to generate the lipid membrane model around the P2X7 receptor ion channel [61]. The information on the lipid bilayer composition is shown in Supplemental Fig. 2 [62].

2.4.3. Molecular docking

Physalin derivatives and P2X7 receptors were studied by molecular docking using the program Molegro Virtual Docker (MVD) 6.0 (CLC Bio, 8200, Aarhus, Denmark) [63]. The MolDock score [GRID] algorithm with a grid resolution of 0.30 Å was used. We optimized the search using the algorithm MolDock Optimizer. The partial atom charges were assigned according to the MVD charges scheme, and the search space was applied around the cavities of the P2X7 receptor [47,48,64,65]. The binding poses were selected according to the best MolDock score.

2.4.4. Molecular dynamics simulations

Molecular dynamics simulations were performed using the program GROMACS 2019 [66]. The program CHIMERA 1.13.1 was used to generate a representation of molecular complexes [67]. A rectangular water box with the protein inserted into a bilayer membrane generated by the CHARMM-GUI server was used for the molecular dynamic

Table 1
Parameters used in the bilayer lipid membrane preparation.

Molecules	Upper leaflet (# of lipids)	Lower leaflet (# of lipids)	Surface area (nm^2)	
Water Thickness	–	–	–	35 nm
CHL1	38	38	40.0	12.93%
POPC	138	138	68.3	46.94%
POPE	76	76	58.8	25.86%
POPS	6	6	60.4	2.04%
SAPI	30	30	67.4	10.20%
PSM	6	6	55.4	2.04%

simulations (Table 1) [68]. The ligand topology was made by CGenFF using the ParaChem server [69].

The steepest descent algorithm made the complex minimization. For equilibration, the bond lengths with hydrogen atoms were constrained by the LINCS algorithm [70]. Particle Mesh Ewald (PME) was used for long-range electrostatic interactions with a real-space cutoff of 12 Ä, and the same cutoff distance was adopted for van der Waals interactions [71].

The system was established using two amounts of substance (N), volume (V), and temperature (T) (NVT) simulations for 500 ps at 303.15 K. Then was used four amounts of substance (N), pressure, and temperature (T) (NPT) simulations for 1000 ps at 303.15 K and pressure at 1 bar using a v-rescale algorithm and Berendsen barostat [72,73]. Finally, the production simulation was made in NPT assemble, for 200 ns, 303.15 K, 1 bar, V-rescale, and Parrinello-Rahman barostat [74] PME and van der Waals real-space cutoff of 10 Timestep in all simulations was set as 2 fs and simulated data saved every 10 ps.

The functions gmx_hbound, gmx_gyrate, gmx_rms, and gmx_rmsd were used to generate the hydrogen bonds, a radius of gyration, Root Mean Square (RMS), and Root Mean Square Deviation (RMSD) graphs, respectively. MM-PBSA (Molecular mechanics Poisson–Boltzmann surface area) was applied to calculate the binding free energy after stabilizing the complex [75]. The tool considers conformational variations along a trajectory. We considered only the last 5 ns of each dynamics to calculate only the portion of the dynamics where the system would be more stable. The two-dimension (2D) intermolecular interaction maps were made using the program Discovery Studio (Dassault Systèmes, BIOVIA).

3. Results

3.1. In vitro assays

3.1.1. P2X7 receptor inhibition evaluated for dye uptake assay

ATP-induced dye uptake assay was used for evaluating the inhibitory activity of *P. angulata* crude leaves ethanolic extract on P2X7 receptor function. Mice peritoneal macrophages did not uptake PI spontaneously (Fig. 1A1) after continuous exposition for 20 min. The treatment with 5 mM ATP induced expressive membrane permeabilization and PI uptake 20 min after treatment (Fig. 1A2). BBG (1 μM) inhibited the ATP effect when preincubated for 5 min (Fig. 1A3). The *P. angulata* crude leaves ethanolic extract preincubated for 5 min reduced ATP-induced PI uptake in 100 ng/mL (Fig. 1A4) and 1 μg/mL (Fig. 1A5). The plant extract dose-dependently inhibited the pore formation with an IC_{50} value of 157 ng/mL (Fig. 1B and C). No concentrations (1 ng/mL to 100 ug/mL) of *P. angulata* crude leaves ethanolic extract induced PI uptake spontaneously (gray bars, Fig. 1B).

The leading group of compounds originating from *P. angulata* crude leaves ethanolic extract purification is the physalin, which possesses 53 distinct types isolated from Physalis [76] with a high diversity of

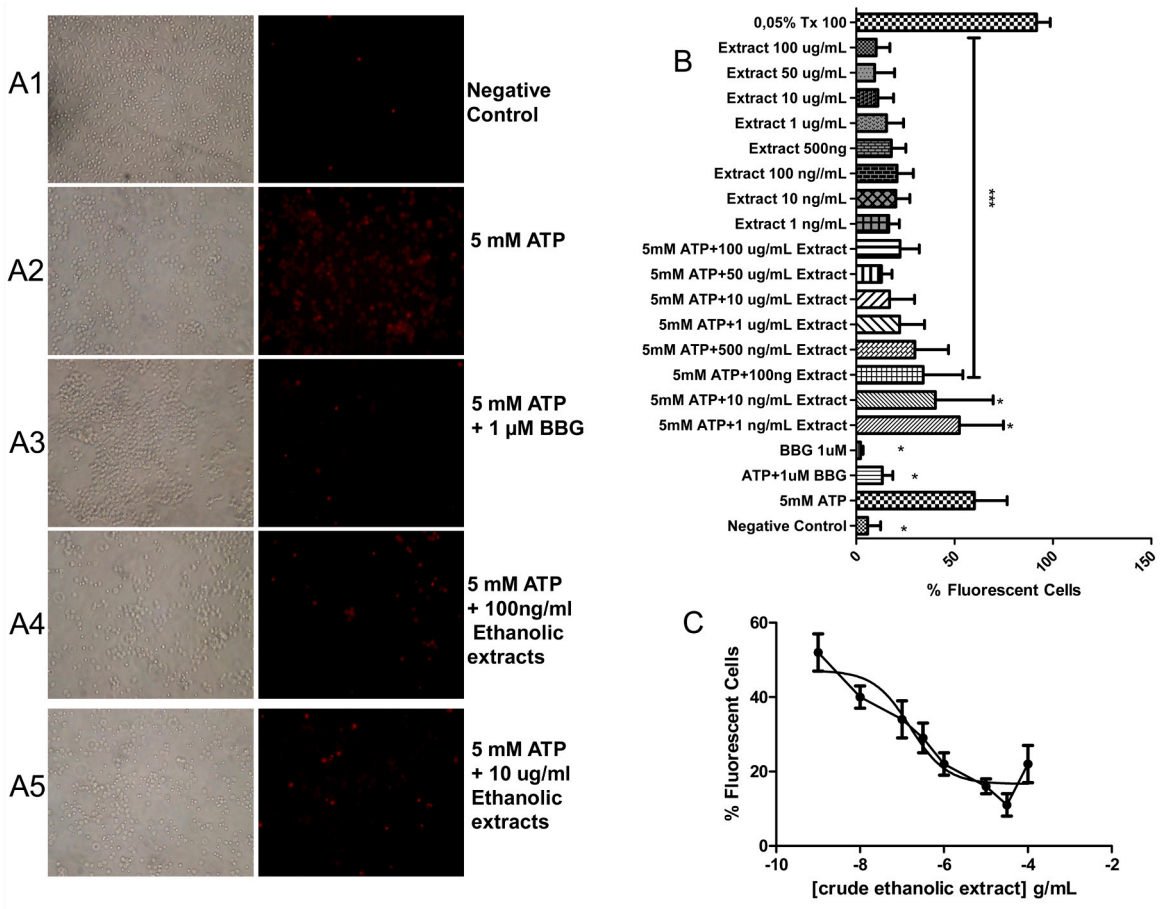

Fig. 1. Inhibitory effect of *P. angulata* crude leaves ethanolic extract on P2X7 activity evaluated by fluorescence microscopy (left panels) and flow cytometry (right panels, bottom). Mice peritoneal macrophages were maintained at 37 °C before the experiment. (A1) No treated cells; (A2) ATP (5 mM); (A3) ATP + BBG (1 μM); (A4) ATP + ethanol extract (100 ng/mL); (A5) ATP + ethanol extract (10 μg/mL); (B) PI uptake assay of macrophages pretreated with crude ethanolic extracts for 5 min before ATP addition (white bars) or no (gray bars); (C) Dose-response curves, in flow cytometry assay, for the ethanol extract in the presence or absence of 5 mM ATP. The values for the total percentage of 0.05% Triton X-100 fluorescence are represented as the mean ± s.d of the total effect. This graph is representative of 3–5 independent experiments in triplicates.

structures. We used a concentrated ethanolic extract from *P. angulata* (CEEPA), rich in physalins B, D, F, and G [77]. All physalins isolated from *P. angulata* use physalin B as a biogenetic precursor. Physalins D, F, and G possess variations in the presence of a hydroxyl or epoxy group in ring B (C-5 and C-6) (Supplemental Fig. 4) [78]. Therefore, we tested this physalins pool containing B, D, F, and G, in cell permeabilization assay to evaluate the pool inhibitory activity on P2X7 receptor function.

The Physalins D was isolated as pure substances after chromatography and elucidated entirely by comparing its physical data reported in the literature [79]. The melting point uncorrected of the isolated

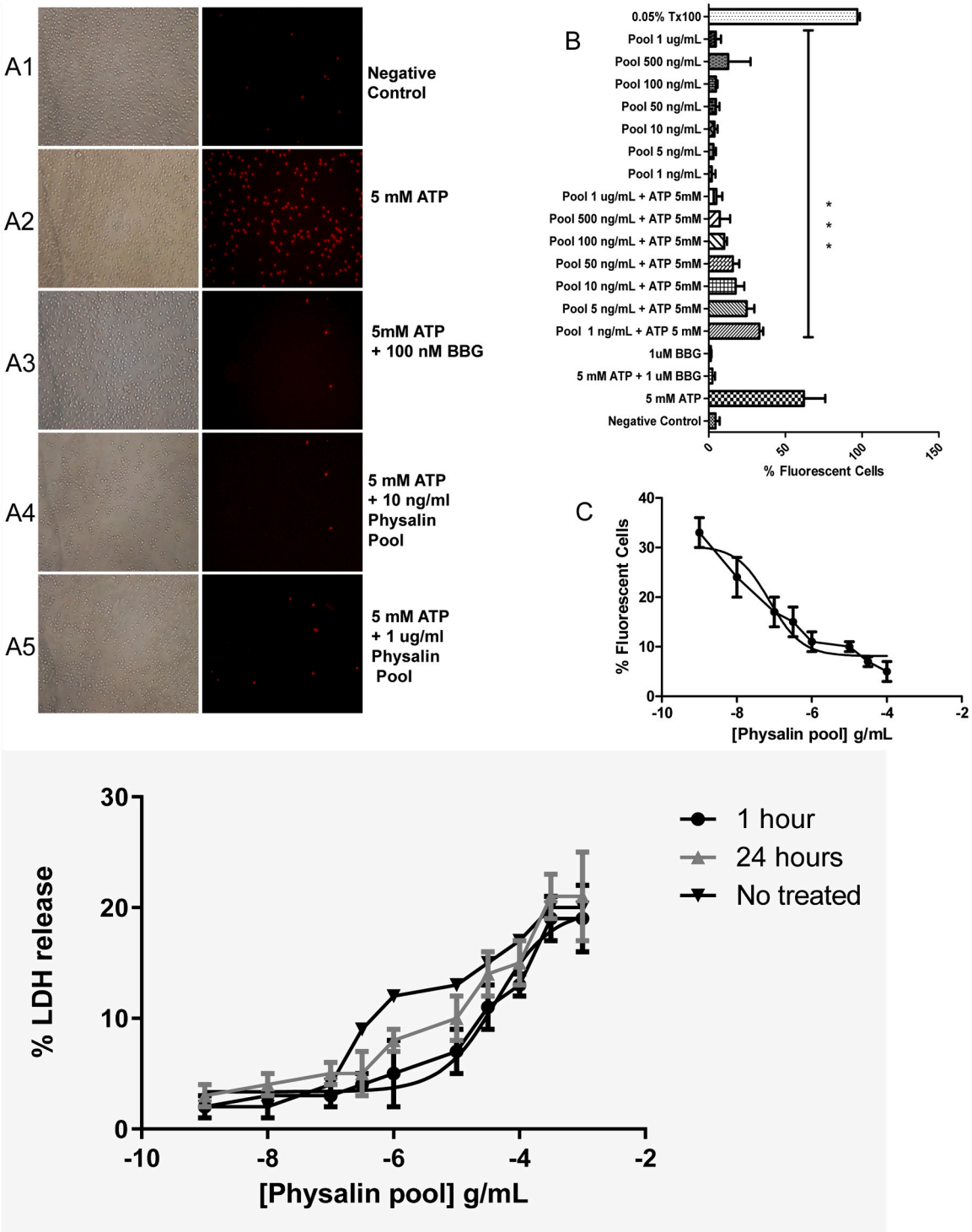

Fig. 2. Inhibitory effect of physalin pool on P2X7 receptor activity. Mice peritoneal macrophages were maintained at 37 °C before the experiment. (A1) No treated cells; (A2) ATP (5 mM); (A3) ATP + BBG (1 μM); (A4) ATP + physalin pool (10 ng/mL); (A5) ATP + physalin pool (1 μg/mL); (B) Dose-response curves, in flow cytometry assay, for the physalin pool in the presence or absence of 5 mM ATP. (C) Dose-response curve of physalin pool concerning LDH release. The black curve represents the LDH release after 1 h of treatment. The gray curve represents the LDH release after 24 h of treatment. The values were normalized about the total percentage of 0.5% Triton X-100-induced LDH release. The values for the total percentage of 0.05% Triton X-100 fluorescence are represented as the mean ± s.d of the total effect. These graphs are representative of 3–5 independent experiments in triplicates.

compound was found to be 284–285 °C. High-resolution ESI-MS mass spectrometry in the negative mode of the isolated compound showed a mass peak of structural ion [M^+, Na^+] at 567, consistent with C28H32O11.

The physalin D FTIR spectrum showed broadband at 3395 cm^{-1}, probably due to the νO-H group. The strong band in 1760, 1729, 1662 cm^{-1} were assigned as νC═O stretching frequency.

The isolate structure substance was also confirmed by the NMR spectral data of the compound by comparing the literature values [79] (). Therefore, to identify the physalin D on the pool using the NMR spectra. In The 13C-N Supplemental Table 1 MR spectrum, the carbons C-5 and C-6 of physalin D appear at 76.3 and 72.5 ppm, respectively, and which differentiate its structure from physalins B, F, and G. In the 1H NMR spectrum, the hydroxyl group (C-5) could also be used to identify physalin D on the pool as shown in the Supplemental Fig. 4.

PLC-UV-DAD analyzed the pool and Physalin D with detection at 225 nm. The mobile gradient phase was accomplished by acetonitrile and water acidified with TFA (0.05% v/v), and the flow rate was 1 mL/min^{-1} in methanol. Quantitative determination was realized by the standard external method based on peak areas. The calibration curve showed good linearity was obtained with $R2 > 0.9997$. The retention time of Physalin D was 33,68 min, with the maximum absorption at 225 nm (Supplemental Fig. 5). A representative chromatogram is presented in Supplemental Fig. 6, showing that physalin D is the highest content (15.2%).

No treated cells were captured, reducing fluorescent dye quantity for cytoplasm (Fig. 2A1). ATP treatment massively increases the dye uptake (Fig. 2A2), and BBG inhibited the ATP effect (Fig. 2A3). Physalin pool preincubated for 5 min in the concentrations of 10 ng/mL (Fig. 2A4) and 1 μg/mL (Fig. 2A5) reversed the ATP-induced PI uptake effect. This inhibitory effect was like BBG inhibition and no treated cells. The physalin pool pretreatment for 5 min dose-dependently inhibited ATP-induced PI uptake (Fig. 2B). The IC_{50} value calculated for the physalin pool was 75 ng/mL (Fig. 2B). The physalin pool cytotoxicity was assessed by measuring LDH release after 60 min and 24 h. The continuous treatment for 1 h caused a maximal LDH release of 19% in the higher concentration tested compared with 0.1% Triton-X 100 (positive control). The treatment for 24 h promoted a maximal LDH release of 21%. No treated cells (cells with crescent solvent DMSO concentrations) produced a basal LDH release level ranging from 2% to 20% after 24 h. Thus, the physalin pool was not cytotoxic for peritoneal macrophages in concentrations until 1 mg/mL (Fig. 2C).

3.1.2. Isolated physalins inhibit P2X7 receptor dye uptake

The physalin potently inhibited the P2X7 receptor activity, as observed in Fig. 2. Additionally, we investigated every physalin individually against P2X7 receptor function. Thus, we confirmed whether every physalin possesses an inhibitory effect on the P2X7 receptor or not. The physalins B, D, F, and G inhibited the ATP-induced dye uptake at a level higher than the BBG antagonist (Fig. 3A1–A8 and Table 2). In addition, physalins D and F were more potent than A740003. Physalin B exhibited IC_{50} like A740003, and physalin G was less potent than A740003 (Table 2). Additionally, when the toxic effect of each isolated physalin was tested, all exhibited a reduced toxic effect with CC_{50} values higher than 900 μg/mL (Fig. 3B and Table 2).

Mice peritoneal macrophages functionally express other P2X receptors associated with dye uptake assay [80]. However, this cellular model for the P2X7 receptor is valid because of the specific pharmacology response associated with the activation of this receptor [81]. Thus, we confirmed the selective P2X7 receptor inhibition evaluating isolated physalins activity against human P2X7 receptor transfected in HEK 293 cells. HEK 293 cells natively did not express P2X receptors.

All isolated physalins inhibited the transfected P2X7 receptor and no caused considerable toxicity (Table 2). Physalin D and F were more potent than A740003 and BBG antagonists to inhibit P2X7 receptor dye uptake. Both substances also were less toxic for HEK-293 cells. This potency and low toxicity were maintained in the mouse P2X7 receptor (Table 2). All physalins exhibit S.I. values higher than the A740003 and BBG antagonist, highlighting physalin D activity against human and mouse P2X7 receptors (Table 2).

3.1.3. Physalins effect on P2X7 receptor macroscopic current

Another relevant function associated with P2X7 receptor activation is the influx of cationic ions after ATP exposition [49]. We realized patch-clamp experiments in whole-cell configuration to determine the physalins effect against the P2X7 receptor-mediated macroscopic currents. ATP (1 mM)-induced current in the presence of increasing physalin B concentrations were dose-dependently inhibited (Fig. 4A) with an IC_{50} value of 102.7 ± 11 ng/mL. All other physalins dose-dependently inhibited the ATP-induced ionic current with IC_{50} values of 12.5 ± 2 ng/mL ng/mL for physalin D, 12.77 ± 1.8 ng/mL physalin F, and 98.68 ± 3.1 ng/mL for physalin G (Fig. 4A). Representative recordings demonstrated the physalin D inhibition, the most potent physalin tested, ATP-induced an ion influx (Fig. 4B1) inhibited after the pretreatment with BBG (Fig. 4B2). Physalin D concentration of 10 ng/mL, 100 ng/mL, and 1 μg/mL dose-dependently reduced the ATP-induced ion influx (Fig. 4B3–B5).

Additionally, we investigated whether the physalins could inhibit the ATP binding in the ATP sites or not in a reversible manner. The dose-response curve for ATP-induced macroscopic current showed an EC_{50} value of 0.522 ± 32 mM. All physalins exhibited similar Km values and distinct plateau values. Physalins diminished the plateau values and higher ATP concentrations to reach the plateau. The treatment with physalins augmented the EC_{50} value for 1273 ± 54 mM (physalin B), 1586 ± 62 mM (physalin D), 1543 ± 43 mM (physalin F), and 0.953 ± 0.04 mM (physalin G). Therefore, physalins inhibited P2X7 receptor function in a non-competitive manner (Fig. 5A–D). Representative recordings demonstrated the 1 μg/mL physalin D effect on crescent ATP concentration (Fig. 5E).

3.1.4. Physalins inhibited ATP-IL-1β and TNF-α release

A hallmark P2X7 receptor function is the capacity of enhancing IL-1β release after the first stimulus with LPS. Additionally, this a relevant cytokine related to pro-inflammatory response. Thus, peritoneal macrophages stimulated with LPS (100 ng/mL) for 4 h and treated with 1 mM ATP in the last 30 min of LPS incubation induced IL-1β release. Physalins, when incubated in the last 60 min of LPS treatment, reversed the ATP effect. Physalin D was the most potent, with an IC_{50} value of 4 ng/mL (Table 3). Compared with A74003, physalin B, D and F exhibited a more potent effect (Table 3). Tumor Necrosis Factor-α (TNF-α) is a major pro-inflammatory cytokine produced in response to macrophages stimulated with LPS via Toll-like receptor 4 (TLR4). Thus, we evaluated the physalin inhibitory activity against ATP- mediated P2X7 receptor activation. All physalins inhibited ATP-induced TNF-α production. Physalin D potently inhibited with 68 ng/mL (Table 3). Like ATP-induced IL-1β release inhibition, physalins B, D, and F were more potent than A74003 to inhibit TNF-α release (Table 3).

3.2. In vivo assays

3.2.1. Physalin D inhibited ATP-induced pleurisy

P2X7 receptors regulate the acute inflammatory response in diverse disease animal models [79]. Additionally, Brustolim and collaborators in 2010 observed physalin F reducing the mice airway inflammation [81,82]. Rathore and colleagues in 2011 using the methanolic leaves extract of *Physalis angulate* described higher inhibitory efficacy when compared to histamine to reverse the anti-histaminic activity by using isolated guinea pig smooth muscle ileum preparation, guinea pig trachea, and rat fundus strip models [83]. Them, we evaluated the isolated physalins capacity of inhibiting the ATP-induced airway inflammatory response. The ATP was administrated in the pleural cavity of mice for 24 h and mediate a response mediated for purinergic receptors.

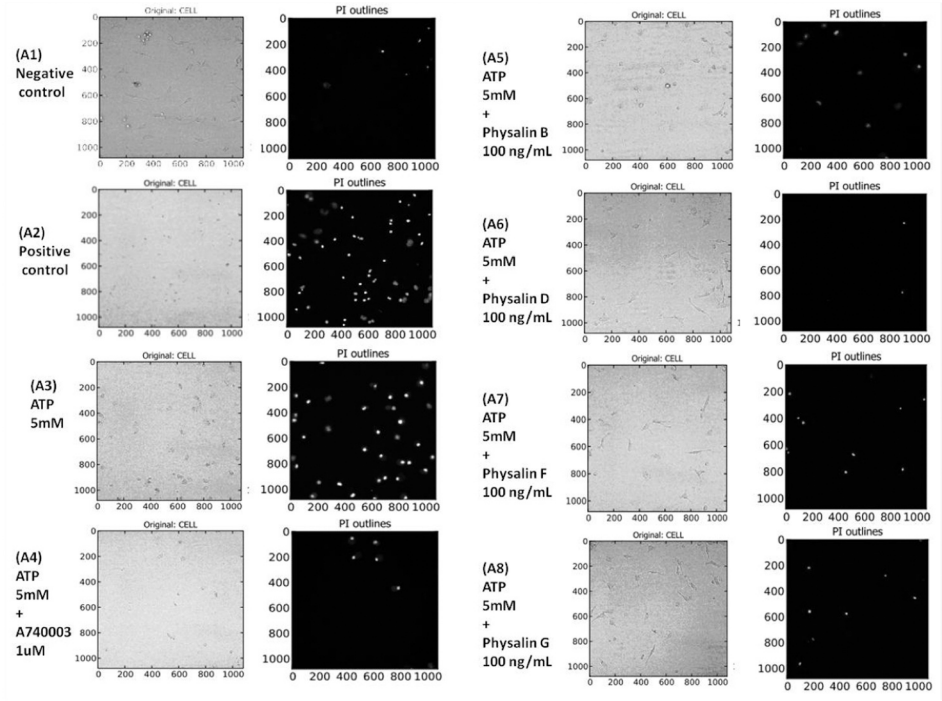

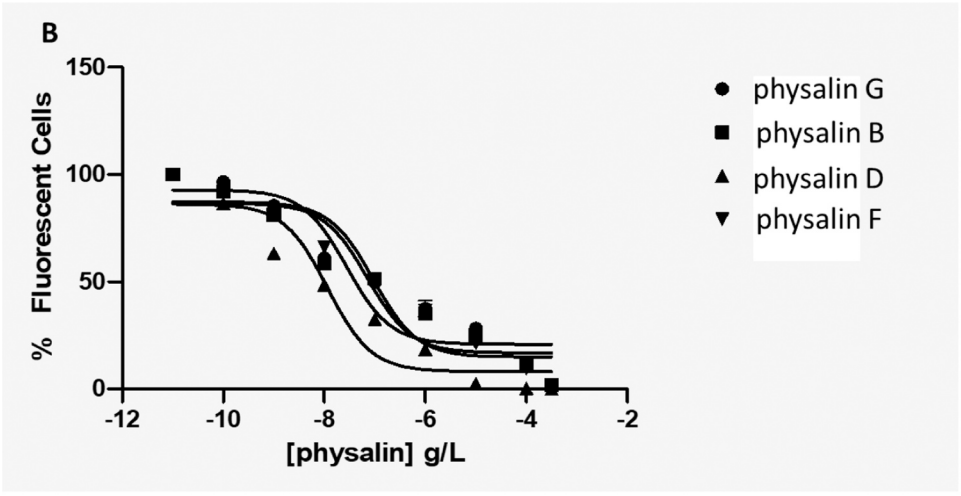

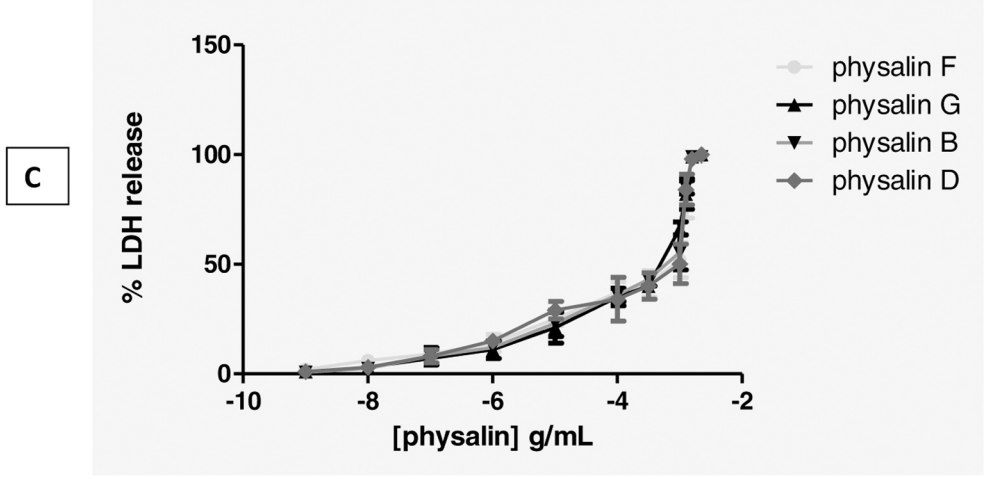

Fig. 3. Inhibitory effect of isolated physalis on P2X7 activity. PI uptake assay of macrophages pretreated with isolated physalins for 5 min before ATP addition. Mice peritoneal macrophages were maintained at 37 °C before the experiment. (A1) No treated cells; (A2) Cells treated with 0.5% Tx100; (A3) ATP (5 mM); (A4) ATP + 1 μM A740003; (A5) ATP + physalin B (100 ng/mL); (A6) ATP + physalin D (100 ng/mL); (A7) (A6) ATP + physalin F (100 ng/mL); (A8) ATP + physalin G (100 ng/mL). (B) Dose-response curve of physalin B, D, F, and G concerning LDH release. The values for the total percentage of 0.05% Triton X-100 fluorescence are represented as the mean ± s.d of the total effect. This figure is representative of 3–5 independent experiments. $P < 0.05$ in comparison with the ATP bar.

Table 2
Inhibitory effect of isolated physalins in HEK-293 cells transfected with human P2X7 receptor and mice peritoneal macrophages.

Antagonists	IC_{50} value HEK-293 transfected with human P2X7 receptor (μM)	CC_{50} value HEK-293 transfected with human P2X7 receptor (μM)	IC_{50} value Mice peritoneal macrophages (μM)	CC_{50} value Mice peritoneal macrophages (μM)	Selectivity index (S.I.) HEK-293 transfected with human P2X7 receptor	Selectivity index (S.I.) Mice peritoneal macrophages (μM)
A740003	0.094 ± 0.05	325 ± 6	0.108 ± 0.14	102 ± 2	3457	944
BBG	0.180 ± 0.33	98 ± 7	0.203 ± 18	112 ± 8	544	551
Physalin B	0.099 ± 7	1033 ± 24	0.133 ± 0.06	989 ± 18	10,434	7436
Physalin D	0.013 ± 3	2144 ± 55	0.047 ± 0.03	2008 ± 41	164,923	42,723
Physalin F	0.054 ± 5	2243 ± 43	0.088 ± 0.05	2094 ± 62	41,537	23,795
Physalin G	0.153 ± 8	1432 ± 33	0.205 ± 0.07	1123 ± 38	9359	5478

IC_{50} values were obtained from concentration-response curves after ethidium uptake assay (*) or propidium uptake assay (**). Data values are expressed as means ± SDs, and all experiments were repeated at least 3 times.

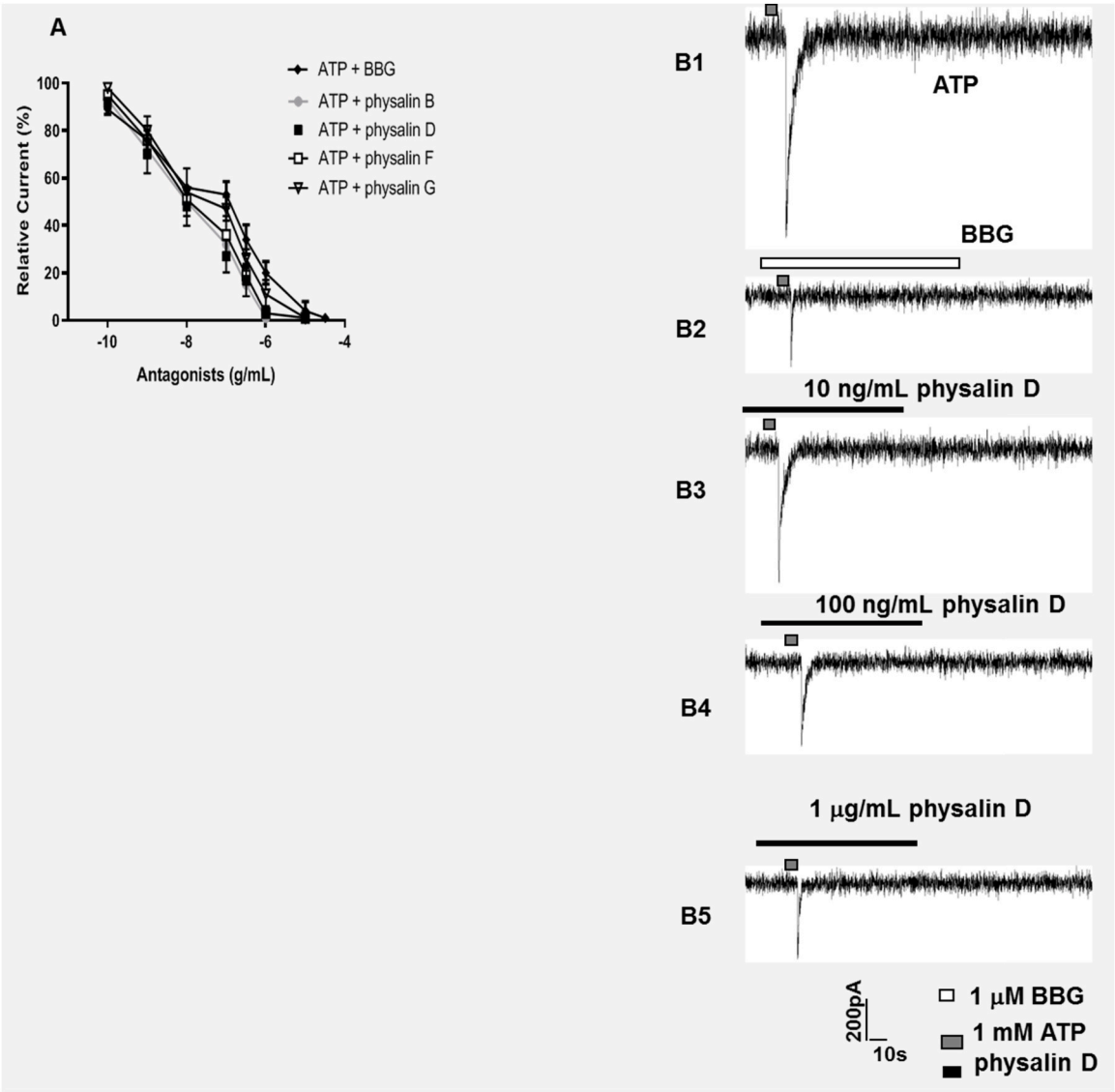

Fig. 4. Physalins inhibit ATP-induced macroscopic currents. (A) Dose-response ATP-induced currents alone or inhibited for 1 μg/mL physalin B, (B) 1 μg/mL physalin D, (C) 1 μg/mL physalin F, and (D) 1 μg/mL physalin G. (E) Representative ATP-induced currents (A1), in crescent concentrations, were inhibited for 1 μg/mL physalin D.All recordings were obtained at 30–37 °C in a holding potential of −60 mV. Graphics are representative of 3–4 independent experiments in triplicates.

Compared to saline administration, ATP treatment increased the mononuclear cells, neutrophils, eosinophils, the quantity extraverted, and IL-1β release in this cavity (Fig. 6). BBG administrated alone did not increase these parameters. When the BBG was administered before the ATP stimulus for 1 h, this P2X7 receptor antagonist reversed the ATP effect, except for the number of mononuclear cells. Glucocorticoid inhibitor dexamethasone also did not interfere in the parameters when treated alone and reversed the ATP-induced responses, except for the number of mononuclear cells. Physalin D exhibited an inhibitory effect for ATP-induced cell migration, protein accumulation, and cytokine release (Fig. 6B–F). This substance did not alter the basal levels when administered alone (Fig. 6).

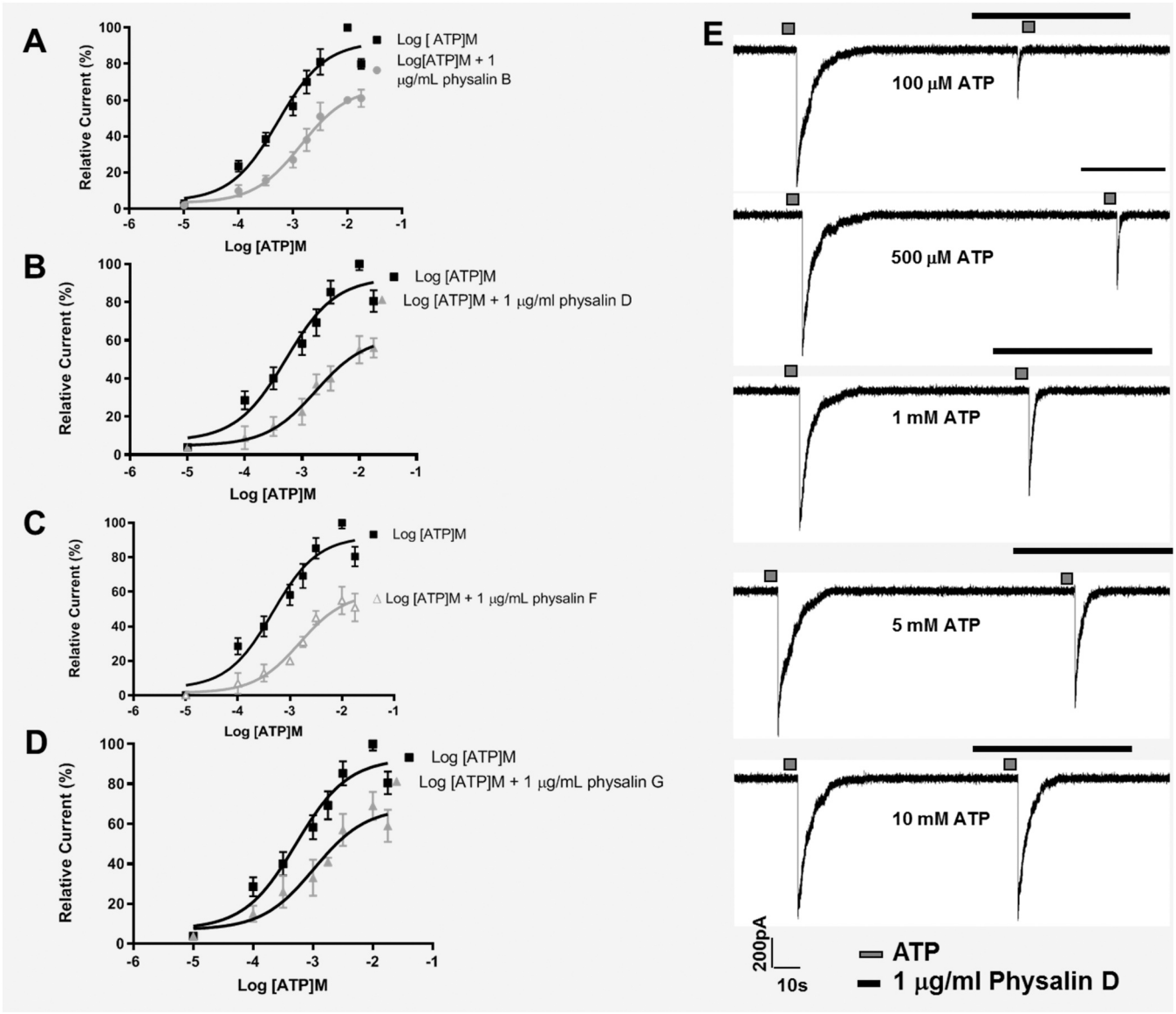

Fig. 5. Evaluation of the inhibitory mechanism of compounds physalins on P2X7 receptor activity. Competitive mechanisms were evaluated by recording the ionic currents of mice peritoneal macrophages with (■) ATP alone or (▲) with 1 μg/mL of physalin B (A), physalin D (B), physalin F (C), and physalin G (D) at 37 °C. (E) Representative recordings show physalin D (1 μg/mL) on macroscopic currents induced for crescent ATP concentrations. Graphics are representative of 3–4 independent experiments in triplicates.

Table 3
Physalins inhibited the ATP-induced cytokines in mouse cells.

Antagonists	IC_{50} value (μM)[a] IL-1β release	IC_{50} value (μM)[a] TNF-α release
A740003	0.090 ± 0.007	0.099 ± 0.008
Physalin B	0.072 ± 0.011	0.089 ± 0.019
Physalin D	0.004 ± 0.0008	0.068 ± 0.09
Physalin F	0.023 ± 0.001	0.085 ± 0.016
Physalin G	0.115 ± 0.017	0.138 ± 0.025

[a] All results represent 3–4 experiments in triplicates at least three different days and are expressed as mean ± s.d.

These results indicate above an ATP-induced P2X7 receptor actuation to recruit inflammatory cells. BBG, physalin D, and dexamethasone pretreatment reversed the ATP effect. Then, we investigated whether physalin D inhibits LPS-induced lung injury and the glucocorticoid receptor (GR) to reduce the inflammatory response. LPS triggered increased total leukocyte and neutrophil numbers, as well as IL-1β levels 24 h after stimulation (Fig. 7). Dexamethasone and physalin D did not alter these parameters when administered alone. Soares and collaborators in 2003 used an LPS-induced acute lung inflammation in mice and did not observe pro- or anti-inflammatory effects caused by RU486, a glucocorticoid agonist [84].

Consequently, we induced the airway inflammation with LPS stimulus and compared the physalin D response with RU486. Thus, we tested the physalin D capacity of reducing the LPS activity and whether this inhibition depends on corticoid pathway inhibition or not. Dexamethasone inhibited the LPS-induced inflammation, and RU486 reversed the dexamethasone inhibition (Fig. 7), as expected for corticoid pathway inhibition. Physalin D reduced the LPS effect, and RU486 did not alter these effects. Therefore, the physalin D inhibited the LPS effect for an independent glucocorticoid receptor pathway (Fig. 7), as previously reported [81].

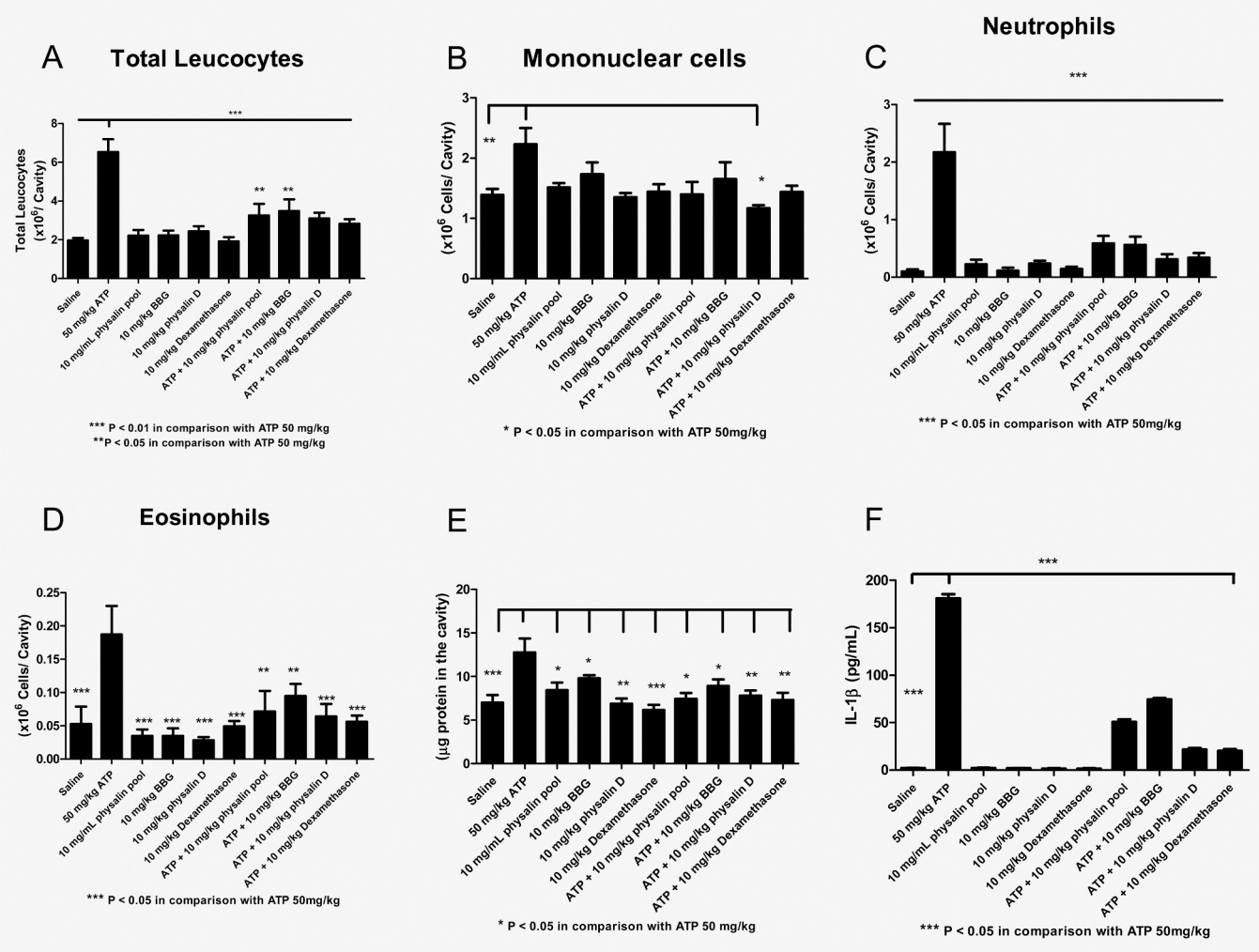

Fig. 6. Effect of physalin D on total cellularity and neutrophil recruitment in ATP-induced pleurisy. (A) Total leukocytes, (B) mononuclear cells, (C) neutrophils, (D) eosinophils, (E) total protein, and (F) IL-1β per pleural cavity of Swiss webster mice orally pretreated (1 h) with physalin D (0.1, and 0.01 mg/kg), dexamethasone and BBG (10 mg/kg), counted under light microscopy 24 h after ATP-challenge. Results are expressed as means ± s.d from at least 4 experiments on different days with three animals for each group.

3.3. *In silico assays*

3.3.1. *Binding mode and binding free energy of physalins*

Molecular dynamics simulations of physalins B, D, F, and G were made to analyze the binding site, RMSD, RMSF, hydrogen bonds, the radius of gyration, and a 2D map of the intermolecular interactions between the protein and the ligands. Additionally, we made binding free energy calculations of the ligands. This data can provide us with information about the affinity of each ligand to the P2X7 receptor.

All ligands (Fig. 8) interacted with the allosteric site, indicating a possible non-competitive inhibition with ATP, the endogenous P2X7 receptor activator.

After the molecular dynamics of 200 ns, the RMSD, RMSF, and hydrogen bonds graphics were made to observe protein-ligands complex behaviors (Supplemental Fig. 6). In the Supplemental Fig. 6A, we can observe a confluence of the graphs, except for physalin B that has less variation in RMSD, indicating that this ligand generated less protein destabilization when compared to other ligands. The Supplemental Fig. 6B, physalins F and G along the trajectory lose their interactions by a hydrogen bond. At the end of the dynamics trajectory, the physalins B and D form hydrogen bonds to the allosteric site residues. There were no significant changes for the radius of the gyration graph in the 4 dynamics trajectory, demonstrating that the mouse P2X7 receptor bonded to the different ligands had the same protein relaxation behavior (Supplemental Fig. 6C).

The RMSF graph (Supplemental Fig. 7) shows how much each residue moved along the trajectory. Three graphs were made concatenating the four physalins dynamics trajectory for each chain of the mouse P2X7 receptor. As a result, this binding is detected in all chains (A, B, and C). We detected peaks in the region of the apical loop of the protein in residues 72–85 and 121–145. These are regions already known for higher movements. Physalin B had the smallest peaks of all, indicating less protein disturbance. Physalin D had the highest peaks in regions close to the allosteric site, indicating a more considerable conformation change of the protein.

We identified the residues interacting with each ligand and the interactions obtained in the final molecular dynamics poses. 2D interaction maps were made for each ligand (Fig. 9). All maps indicated that the ligands bonded to the allosteric site according to interacting residues. For example, physalin B performed pi-stacking interactions with PHE95 from two different chains and with TYR295, hydrogen bond with GLN98, and several hydrophobic interactions with the residues present.

Physalin D made pi-stacking bonds with PHE95 and PHE293 and hydrogen bonds with GLN98 and hydrophobic interactions. Physalin F made several pi-stacking interactions with residues PHE293, TYR295, PHE95 from different chains, and finally, physalin G interacts by pi-

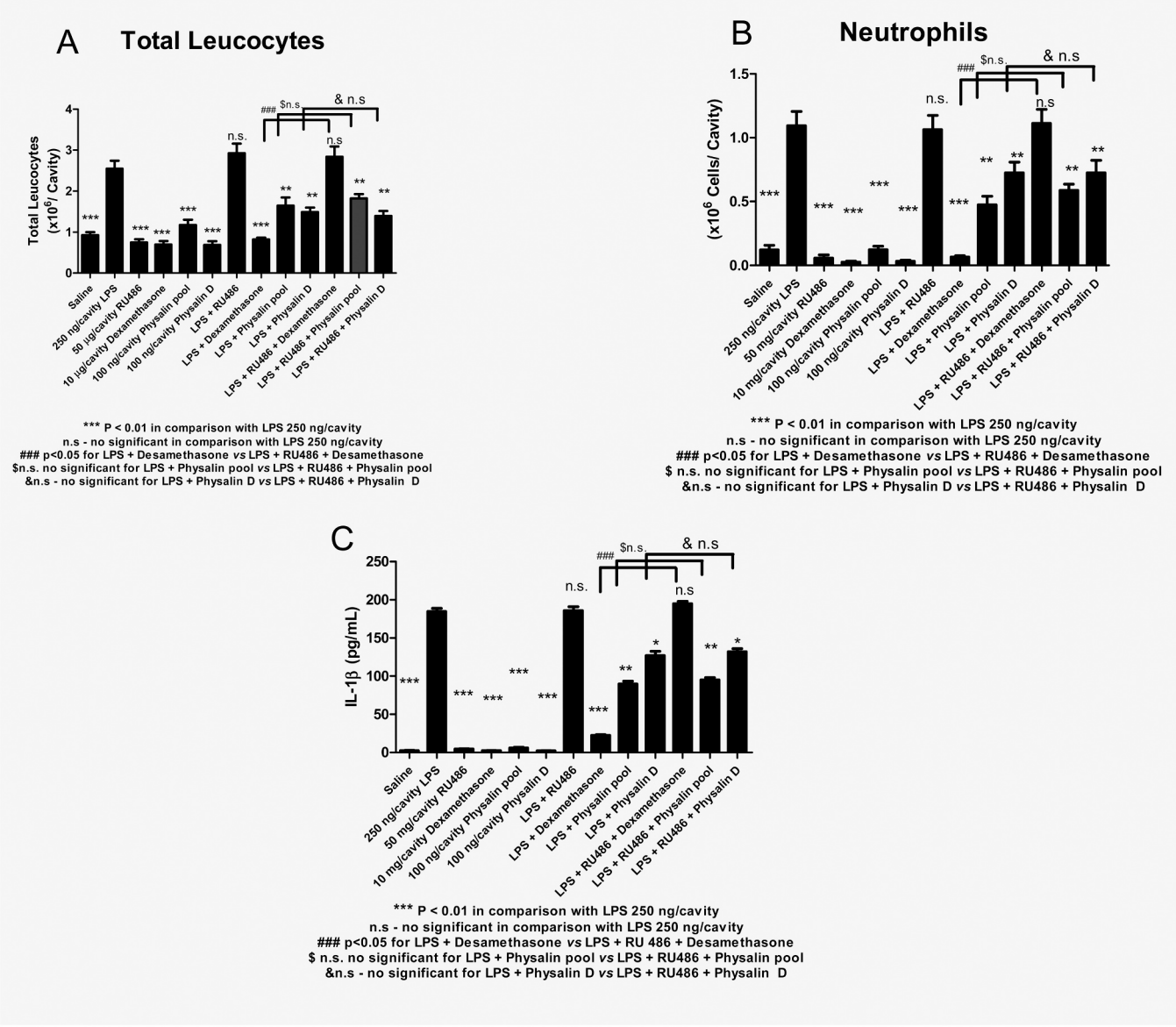

Fig. 7. Effect of physalin D impaired (LPS)-induced pleurisy for a pathway glucocorticoid receptor-independent. (A) Total leukocytes (B) number of neutrophils (C) and IL-1β release per pleural lavage of Swiss webster mice orally pretreated for 1 h with BBG, dexamethasone, and physalin D (0.01, and 0.1 mg/kg), counted under light microscopy 24 h after LPS-challenge. RU486 pretreatment for 2 h before LPS stimulus and consequently 1 h before BBG, dexamethasone, and physalin D. Results are expressed as means ± SD from at least six animals. + Significant difference ($p < 0.05$) from the unchallenged group; * significant difference ($p < 0.05$) from the untreated LPS-challenged group. Statistical significance was determined with one-way ANOVA and a post hoc Tukey test. Results are expressed as means ± SD from 3 to 4 experiments on different days with at least three animals for each group.

stacking with PHE95 and pi-sigma with PHE293.

The last 5 ns of each dynamic trajectory were analyzed with the MM-PBSA tool, which calculates different interaction energies between the ligand and the protein. Their sum gives us the binding free energy, which in short means the ligand affinity to its receptor (Table 4). Physalins G and B had the binding free energy less favorable. Physalin G also made the smallest number of interactions according to the 2D interaction map. Interestingly, physalin B was the least generated protein structural variation in the RMSD and RMSF graphs. On the other hand, physalins D and F had a better result for binding free energy. This result is confluent with a 2D interaction map, where both compounds made a more significant number of intermolecular interactions.

4. Discussion

A large amount of data with new antagonists for the P2X7 receptor have been published. However, the number of publications with natural compounds has been scarce. New antagonists for the P2X7 receptor have been extensively investigated, and some of these candidates are reaching the clinical stage [85]. However, none has approved commercialization for therapeutic purposes.

In general, the pre-clinical and clinical trials involving the P2X7 receptor focus on inhibiting the inflammatory response progression. Acute Lung Injury (ALI) occurs for an uncontrolled systemic inflammatory response from direct injury to the lung or indirect injury in a systemic process milieu.

This complication is related to high morbidity and mortality rates [86,87]. Pharmacological treatments for ALI are insufficient, so discovering new drugs that can inhibit the inflammatory response and alveolar injury can generate a better therapeutic response. Like P2X7 receptor studies, new drugs for ALI derived from natural products do not progress, mainly to discover the mechanism of the compound of action.

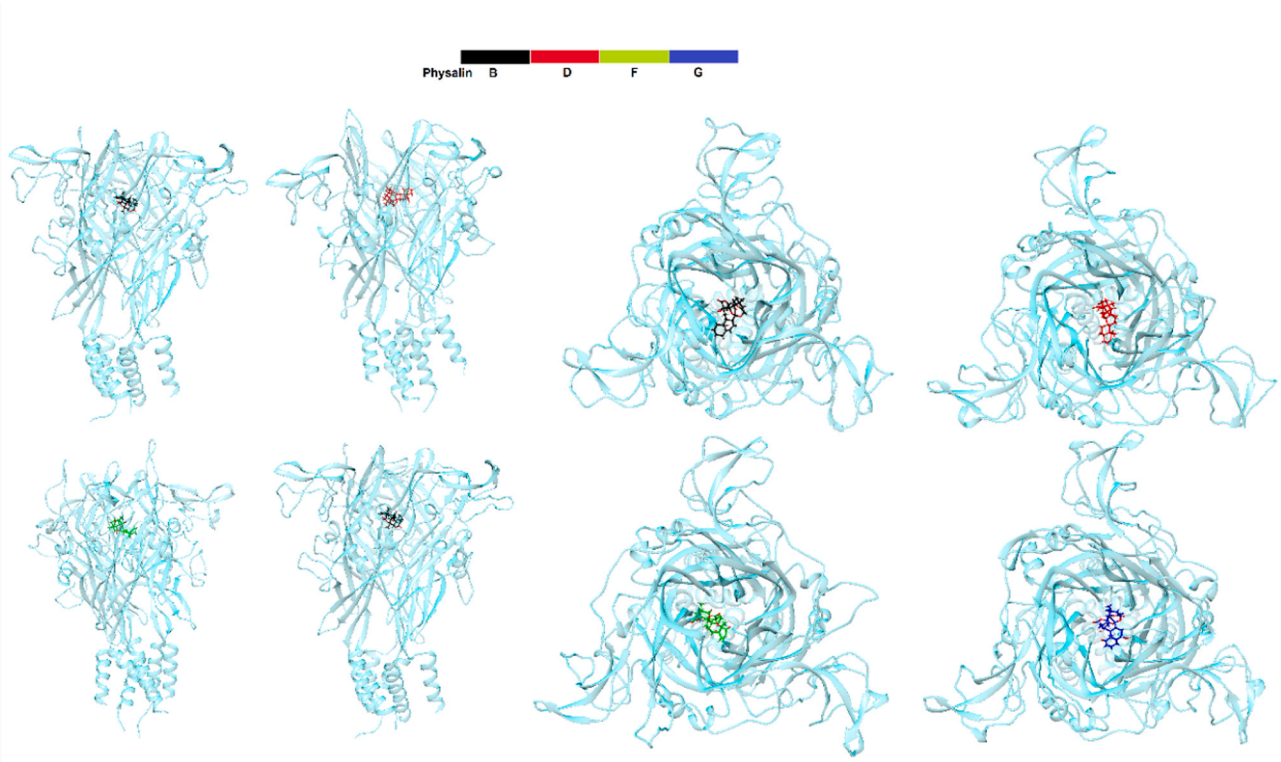

Fig. 8. Binding sites of physalin in mouse P2X7 receptor. Physalin B (black), physalin D (red), physalin F (green), and physalin G (blue). (For interpretation of the references to color in this figure legend, the reader is referred to the web version of this article.)

We studied the action of ethanolic extract, physalins pool, and these isolated physalins from *P. angulata* leave as P2X7 receptor inhibitors in vitro, in addition to anti-inflammatory action on acute inflammatory mice model and e ALI model in mice.

We used a standardized concentrated ethanolic extract from *Physalis angulata* rich in physalins (B, D, F, and G) [88]. Crude ethanolic extract from leaves dose-dependently inhibited ATP-induced dye uptake in nanograms concentration. Interestingly, the crude extract exhibited lower IC_{50} values for reducing ATP-induced dye uptake than other recent publications testing natural product extracts [89,90]. Thus, new studies about this extract may represent novel molecules with a capacity of inhibiting P2X7 receptor function.

Physalin pool containing physalins B, D, F, and G impaired the ATP response reducing the IC_{50} value for inhibiting P2X7 receptor function compared with the crude ethanolic extract. Curiously, Santo and collaborates in 2019 demonstrated the concentrated ethanolic extract with the antinociceptive effect more potent than physalin pool [90]. The authors attributed this result to a synergic effect caused by molecules in the extract. Our assay analyzes the P2X7 receptor function, a receptor associated with inflammatory response promotion, in 2D-monolayer cell type, a system that is simpler than mice nociceptive models. Thus, a reduced number of molecules may be benefitted from interacting with ATP-binding sites or allosteric sites located on the P2X7 receptor.

Physalin pool was not toxic after 1 or 24 h of treatments, as observed for previous acute toxicological experiments in murine using the methanolic extract of *P. angulata* leaves [91] and aqueous extract from roots [92]. Thus both studies did not observe the toxic effects caused by this plant.

The isolated substances (physalin B, D, F, and G) inhibited P2X7 receptor functionality. Physalin D was the most potent to reduce ATP-induced function in primary mice peritoneal macrophages and HEK 293 cells transfected with the hP2X7 receptor in vitro.

The whole-cell patch-clamp assay was realized for investigating the isolated physalin's effect on P2X7 receptor macroscopic currents. All physalins inhibited the P2X7 receptor currents with high potency in comparison to BBG. Furthermore, like previous publications, all isolated physalins reduced P2X7 receptor activity in a non-competitive manner with ATP-binding sites [93]. Interestingly, other isolated substances from natural products did not inhibit the P2X7 receptor function in low nanomolar concentrations, as observed for physalins [42,94,95].

Primary cells as rat and mice peritoneal macrophages and cellular lineages as J774, RAW 264.7, and activated THP-1 cells express P2X7 receptors and are used as a functional cellular model. These cell types natively express more than one purinergic receptor subtype, in particular the P2X subtype. However, lineages as HEK-293 did not express native P2X receptors. Thus, the P2X7 receptor may be transfected for measuring a more selective result. Fischer and collaborators screened a compound library of about 2300 biologically active and selected 800 different molecularly defined natural compounds. HEK293 cell line stably expressing human P2X7 in an ATP (1 mM) model-induced Ca^{2+} response was blocked for teniposide at sub-micromolar concentrations. Physalin B, D, F, and G inhibited macroscopic currents on mice peritoneal macrophages and dye uptake on macrophages and HEK293-transfected with P2X7 receptor. The physalin B, D, and F inhibitory activity were like to report for teniposide. In this same publication, agelasine (AGL) and garcinolic acid (GA) facilitated the P2X7 receptor Ca^{2+}-response to ATP. GA increased the YO-PRO-1 uptake, whereas AGL did not affect the ATP-stimulated intracellular accumulation of this dye [96].

Australian marine sponge *Stylissa flabellata* yielded two new bisimidazo-pyrano-imidazole bromopyrrole ether alkaloids, stylissadines A (IC_{50} = 0.7 μM) and B (IC_{50} = 1.8 μM), as P2X7 receptor antagonists [42] evaluated for dye uptake assay. However, both substances were less potent than physalin B, D, F, and G.

Rhein (4, 5-dihydroxyanthraquinone-2-carboxylic acid) is a rhizome of rhubarb, a traditional Chinese herb. Rhein inhibit ATP/2′(3′)-O-(4-Benzoylbenzoyl)adenosine 5′-triphosphate (BzATP)-induced [Ca2+]c increase in HEK-293 transfected cells (IC_{50} = 1.31 μM), rat peritoneal

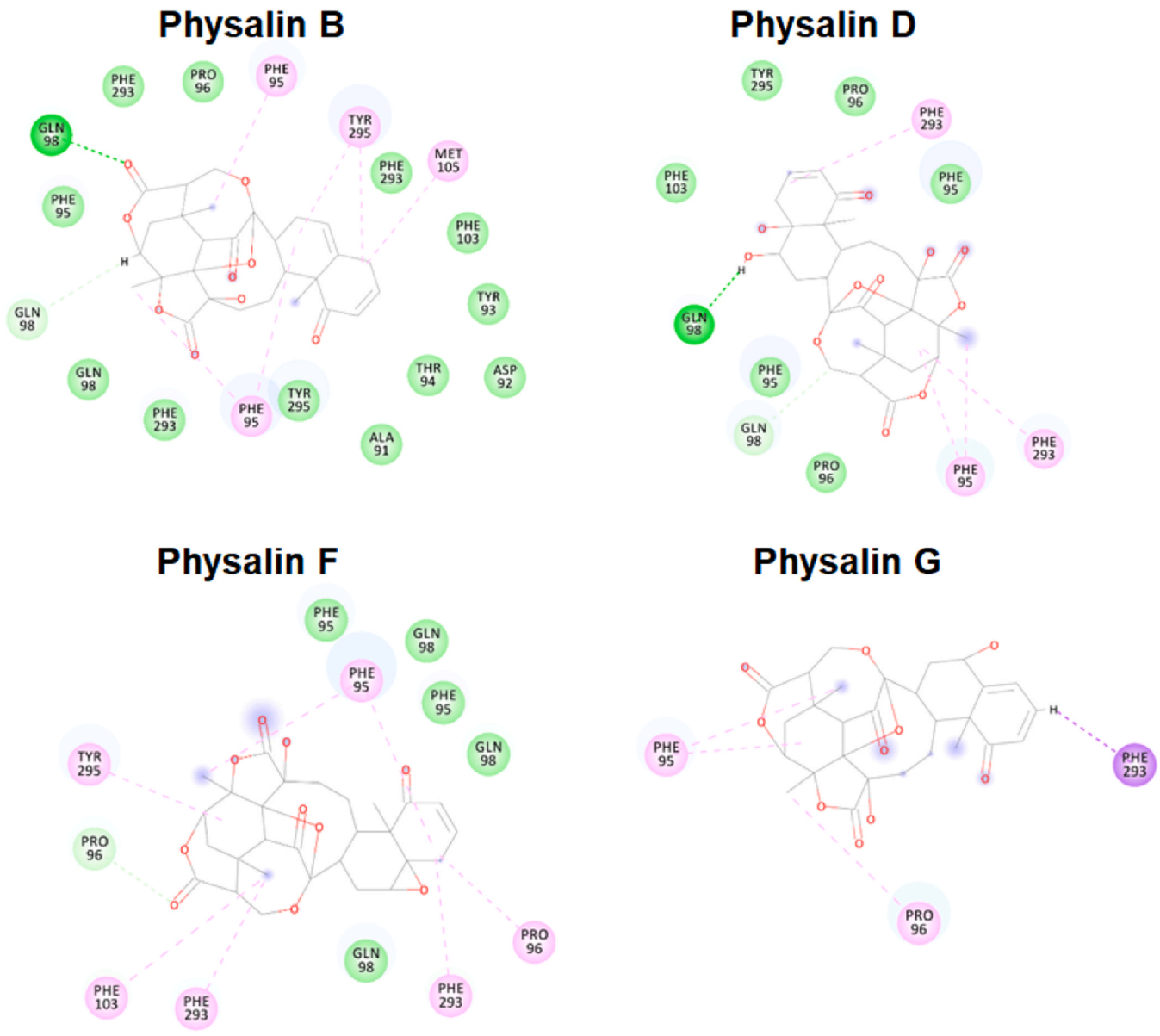

Fig. 9. Intermolecular interactions of physalins B, D, F, and G to mouse P2X7 receptor.

Table 4
Binding free energy calculation between ligands physalins and P2X7 receptor protein performed during the last 5 ns from molecular dynamics simulation trajectory using the MM-PBSA method.

Energy (kJ/mol)	Physalin B	Physalin D	Physalin F	Physalin G
van der Waals	−177.652	−163.912	−169.427	−153.173
	+/−6.289	+/−10.144	+/−4.788	+/−8.620
Electrostatic	−19.061	−20.638	−9.004	−13.966
	+/−5.250	+/−9.121	+/−5.976	+/−5.267
Polar solvation	127.912	92.589	81.846	98.057
	+/−11.622	+/−6.917	+/−8.324	+/−8.547
SASA[a]	−21.356	−19.408	−19.167	−19.380
	+/−0.644	+/−0.888	+/−0.562	+/−0.973
Binding Free Energy	−90.158	−111.369	−115.751	−88.462
	+/−14.633	+/−8.369	+/−7.274	+/−8.707

[a] SASA = Solvent accessible surface area.

macrophages (IC_{50} = 0.49 μM), pore formation (IC_{50} = 1.04 μM), ROS production (IC_{50} = 1.56 μM), IL-1β release (IC_{50} = 1.48 μM) and cell apoptosis (IC_{50} = 0.4 μM) by antagonizing the P2X7 receptor in rat peritoneal macrophages [97]. Thus, all physalins were more potent than Rhein to inhibit the P2X7 receptor function in vitro in all assays evaluated.

Emodin (1,3,8-trihydroxy-6-methylanthraquinone), an anthraquinone derivative isolated from *Rheum officinale* Baill reduced ATP-induced macrophage death with IC_{50} of 0.2 μM. ATP-induced dye uptake and BzATP-induced intracellular Ca^{2+} increase were inhibited with an IC_{50} of 0.5 μM. Furthermore, emodin significantly suppressed BzATP-evoked currents in P2X7 receptor-expressing HEK293 cells with an IC_{50} of 3.4 μM [98]. Additionally, emodin suppressed the ATP-induced IL-1β release with an $IC_{50}$of 1.6 μM, ROS production and phagocytosis attenuation triggered by ATP, with IC_{50} values of 1 μM and 0.7 μM [99]. All physalins exhibited better potency to reduce P2X7 receptor functions in comparison to emodin.

IL-1β release and TNF-α were inhibited in mice P2X7 receptors. All physalins inhibited both cytokines release in nanomolar concentrations. Physalin G, when compared with BBG, was slightly less potent. However, physalin B, D, and F showed better inhibitory activity than BBG. Physalin D was highly potent in inhibiting with an IC_{50} value almost in subnanomolar concentration. This data was compared to a previous

publication [78] and is a relevant detail. In general, isolated substances from natural products possess low cytokine inhibition mediated by P2X7 receptor activation [98,100,101].

ATP-induced edema was evaluated in mice paws. Physalin B, F, and G poorly reversed the ATP-induced edematogenic effect compared with BBG (data not shown). In contrast, physalin D inhibited the edematogenic response with more potency than A740003. The inhibition range remained in the nanomolar scale, as observed in in vitro assays. This result was observed for previous publications with synthetic drugs inhibiting P2X7 receptor activity in a similar animal model [64,65,98,100,101]. The higher physalin D hydrophilicity may explain the discrepant superior in vivo activity when compared with other physalins.

Interestingly, the inhibitory activity level observed in vitro for physalin B, F, and G was maintained in vivo. Physalin F and physalin B showed similar performances, with physalin F better than physalin B. Physalin G conserved the worse effect. Thus, physalin B and F could be a scaffold for new hydrophilic prototypes with the capacity of inhibiting P2X7 receptors in vitro and the inflammatory response in vivo. The expressive effect in nanograms per kilo, when compared with other physalins, highlighted physalin D for subsequent in vivo assays.

Interestingly, complete Freund's adjuvant (CFA)-induced paw inflammation in mice was not inhibited for intraperitoneal treatment of B, D, and G physalins after 2–6 h of exposition. Physalin G reduced this inflammatory response and IL-1β release in the concentration of 100 mg/kg [102]. All physalins were effective in reducing the central nociceptive effect induced for CFA. In rats, a CFA-induced orofacial pain model for 5 days, the CFA was administered subcutaneously to the vibrissa pad. The P2X7 receptor antagonist 3-[[5-(2,3-Dichlorophenyl)-1H-tetrazol-1-yl]methyl]pyridine hydrochloride (A438079) added intracisternal caused anti-hyperalgesic effects against thermal stimuli compared to the vehicle group [103]. This result paves the way for further studies on the physalin mechanisms of central and inflammatory pain inhibition. However, the discrepancy of physalin D activity with the CFA model [102] should be investigated.

Physalin D is the most hydrophilic molecule of this pool [89]. Therefore, the possible significant extracellular concentration may explain the higher potency than other physalins and a higher facility to solubilize and eliminate the metabolism. Physalin D tissue pharmacokinetics and distribution studies in rats after intravenous administration (2 mg/kg) demonstrated a rapid elimination without detection after 200 min of administration. This short t1/2 was attributed to fast tissue distribution, possible rapid metabolic conversion, and preferential excretion by the kidney [90]. Oral administration of 25 mg/kg of physalin D in rats confirmed the fast conversion and excretion for urine and feces [89]. Thus, physalin D may be a prototype for new synthetic improvements.

Neutrophil recruitment in inflammatory pathogenesis associated with acute lung injury [103,104]. ATP accumulation inhibition may block the late, but not the early, neutrophil recruitment stages to the lung after LPS administration. Moreover, after 24 h of LPS stimulus, the ATP presence augments the cellularity, neutrophils, and protein concentration in the bronchoalveolar lavage fluid (BALF) [101]. Monção-Ribeiro reported P2X7 receptor participation in mice LPS-induced lung injury. Wild-type (C57BL/6) mice augmented lung inflammatory parameters, the influx of polymorphonuclear and Cluster of differentiation (CD)14+ cells, and IL-1β release after LPS stimulus for 24 h. P2X7 knockout (KO) mice attenuated all these parameters [105].

Thus, we administered ATP in the pleural cavity for 24 h. This stimulus caused cellularity recruitment and total protein and pro-inflammatory cytokines release. However, all parameters were impaired for BBG, and especially for physalin D treatment.

Matsuyama and collaborates attributed the P2Y2 receptor, the ATP-induced acute inflammatory effects in mice lung [106]. We ruled out this possibility using the P2Y2 receptor antagonist 5-[[5-(2,8-Dimethyl-5H-dibenzo[*a*,*d*]cyclohepten-5-yl)-3,4-dihydro-2-oxo-4-thioxo-1(2H)-pyrimidinyl]methyl]-N-2H-tetrazol-5-yl-2-furancarboxamide (AR-C 118925XX,10 mg/kg) before the ATP stimulus. However, we did not observe inhibition (data not shown).

Emodin treatment was used in asevere acute pancreatitis (SAP) model in rats through Nucleotide oligomerization domain (NOD)-like receptor protein 3 (NLRP3) inflammasomes. SAP model group evoked by a conventional reverse infusion of 5.0% sodium taurocholate into the biliopancreatic duct in 30 mg/kg and 60 mg/kg for emodin-treated groups. SAP altered the plasma amylase, lipase, IL-1β, interleukin-18 (IL-18), myeloperoxidase (MPO) activities, pathological scores of pancreases, and the expression levels of P2X7 receptor. On the other hand, emodin (60 mg/kg) could impair the pancreatic histopathology and acinar cellular structure injury, downregulate the plasma amylase and lipase levels, MPO activities in pancreatic tissues, and impaired the P2X7/NLRP3 activation followed by the decrease of pro-inflammatory factors [107]. Although the emodin results are auspicious, the physalin D data inhibited the acute inflammatory response in concentrations 6 times inferior to emodin. Alternatively, physalin D may be considered an alternative for severe acute pancreatitis treatment.

LPS has induced ALI/Acute respiratory distress syndrome (ARDS) in animal models [108]. Additionally, Elevated ATP levels in BALFs are found after 24 h of LPS exposition in mice. A phenotype commonly associated with the pathogenesis of ALI [106,109]. Complementary, the ATP-induced lung inflammatory response was inhibited for dexamethasone treatment.

Thus, we treated the mice with LPS 24 h to verify the physalin D effects in this characteristic acute lung injury animal model. LPS promoted cellularity recruitment, as expected, and cytokine increase. P2X7 receptor antagonists reduced this effect, correspondingly to the physalin D pretreatment. This reversion in the LPS effect was similar to describe for Monção-Ribeiro in 2011 using KO P2X7 receptor mice [105]. Additionally, carrageenan-induced pleurisy was reversed for BBG in mice [110]. These data indicate P2X7 receptor participation in LPS-induced lung injury and physalin D capacity to inhibit mice effect. Interestingly, the physalin D effect occurred in a manner independent of the glucocorticoid pathway.

Collagen-induced arthritis in BALB/c mice produced paw edema and joint inflammation when compared to vehicle-stimulated. Oral physalin F and dexamethasone treatment inhibited the collagen effect. COS-7 transfected with a plasmid encoding for a yellow fluorescent protein (YFP)-GR fusion protein in vitro indicated predominant cytoplasm YFP staining after dexamethasone treatment, in contrast to physalin F treatment with YFP staining was concentrated in the nuclei. Thus, the authors dedicated the physalin F immunosuppressive activity mechanism distinct from glucocorticoids [111].

Ding and collaborates in 2019 described LPS-induced pro-inflammatory effects in mice inhibited for physalin D treatment. This inhibition was attributed to the physalin D-mediated regulation of macrophage M1/M2 polarization via signal transducer and activator of transcription (STAT) [112]. Although we did not show, the physalin D also reversed mononuclear cells after LPS stimulus.

The absence of drugs to treat ALI/ARDS associated with the prevalence and mortality observed for these disorders highlights the results of physalin D. We observed that physalin D inhibits the P2X7 receptor in vitro ATP-induced edematogenic response via the P2X7 receptor in vivo. The ALI model induced by ATP and LPS was reversed by A74003 and physalin D inhibiting the P2X7 receptor. The inhibition occurred without interfering with the glucocorticoid pathway. Interestingly, *Physalis angulata* may exert anti-inflammatory effects using pathways cyclooxygenase dependent or not [25]. Therefore, the action of physalin D reducing the formation of edema, cell recruitment, and secretion of cytokines are relevant factors for ALI treatment. This reversal mainly targets the P2X7 receptor, highly expressed in type I alveolar cells (AEC I) [113].

Additionally, this receptor is related to cell death induced by BzATP in AEC I cells [114]. Therefore, the P2X7 receptor activation may be one

of the factors associated with AEC I damage, leading to the deficiency of gas exchange and disruption of fluid clearance observed in ALI induced by different factors [115–119]. Therefore, the anti-inflammatory action independent of receptors for glucocorticoids may represent the expectation of reduced or absent adverse effects, especially long-term treatments.

Binding Free Energy Calculation between ligands physalins and P2X7 receptor indicates a fair value of all physalins interaction. Additionally, all physalins interact in the P2X7 receptor allosteric binding site. Physalin D and F exhibited the most favorable binding free energy values.

In the function of a low effective alternative to treat ALI and ARDS, the physalin D shows effective anti-inflammatory activity, low murine toxicity, good aqueous solubility and pharmacokinetics of absorption, low liver conversion and fast and high urine and fecal excretion. All these parameters represent physalin D as a promisor substance to clinical studies.

5. Conclusions

Physalin B, D, and F are potent and promisor mice and human P2X7 receptor antagonists. However, physalin G always exhibited worse activity than BBG or A740003. Although all physalin B, D, F, and G may binding to allosteric ATP sites. Physalin D and F bound to P2X7 receptor allosteric cavity with low free-biding energy. A data compatible with higher potency to inhibit the P2X7 receptor was observed at in vitro assays. Physalin D potently reversed the ATP-induced edematogenic response in mice. However, other physalins, possibly because of low hydrophilicity inhibited with doses more than 100 times inferior to physalin D. ATP and LPS-induced lung inflammation were inhibited for glucocorticoid, as expected, BBG and physalin D. Physalin D reduced the cellularity in a level like a dexamethasone, however using a pathway independent of the glucocorticoid receptor. All data mentioned above associated with low toxicity and satisfactory pharmacokinetics support physalin D as a promising candidate to ameliorate inflammatory states through P2X7 receptor inhibition, focusing on ALI and ARDS treatment.

Funding

This work was supported by CNPq (National Council of Research of Brazil) (RXF holds a grant with Fellowship Process Number 308755/2018-9), CP holds a grant from the Brazilian agency CNPq. FAPERJ (Research Support Foundation of the State of Rio de Janeiro) (JCNE (Young Scientist from Our State) with Fellowship process number E-26/203.246/2017) and Emergent Group of Research from Rio de Janeiro (E-26/211.025/2019) for the financial support, and to CAPES (Coordination for the Improvement of Higher Education personnel) for the support through scholarships.

CRediT authorship contribution statement

J.C.C. Arruda: Methodology, Development or design of methodology; creation of models, investigation, Conducting a research and investigation process, specifically performing the experiments, or data/evidence collection. **N.C. Rocha:** Methodology, Development or design of methodology; creation of models, investigation, Conducting a research and investigation process, specifically performing the experiments, or data/evidence collection. **E.G. Santos:** Methodology, Development or design of methodology; creation of models, Software, Programming, software development; designing computer programs; implementation of the computer code and supporting algorithms; testing of existing code components, investigation Conducting a research and investigation process, specifically performing the experiments, or data/evidence collection, Visualization, Preparation, creation and/or presentation of the published work, specifically visualization/data presentation. **L.G.B. Ferreira:** Conceptualization, Ideas; formulation or evolution of overarching research goals and aims, Software, Programming, software development; designing computer programs; implementation of the computer code and supporting algorithms; testing of existing code components, investigation Conducting a research and investigation process, specifically performing the experiments, or data/evidence collection, Visualization Preparation, creation and/or presentation of the published work, specifically visualization/data presentation. **M.L. Bello:** Conceptualization, Ideas; formulation or evolution of overarching research goals and aims, Software, Programming, software development; designing computer programs; implementation of the computer code and supporting algorithms; testing of existing code components, Validation – Verification, whether as a part of the activity or separate, of the overall replication/reproducibility of results/experiments and other research outputs, Writing – original draft, creation and/or presentation of the published work, specifically writing the initial draft (including substantive translation), Writing – review & editing, Preparation, creation and/or presentation of the published work by those from the original research group, specifically critical review, commentary or revision – including pre-or postpublication stages, Visualization, Preparation, creation and/or presentation of the published work, specifically visualization/data presentation. **C. Penido:** Conceptualization, Ideas; formulation or evolution of overarching research goals and aims, Methodology, Development or design of methodology; creation of models, Validation - Verification, whether as a part of the activity or separate, of the overall replication/reproducibility of results/experiments and other research outputs, Writing – original draft, Preparation, creation and/or presentation of the published work, specifically writing the initial draft (including substantive translation), Writing – review & editing, Preparation, creation and/or presentation of the published work by those from the original research group, specifically critical review, commentary or revision – including pre-or postpublication stages. **T.E. M.M. Costa:** Conceptualization, Ideas; formulation or evolution of overarching research goals and aims, Methodology, Development or design of methodology; creation of models, Writing – original draft, creation and/or presentation of the published work, specifically writing the initial draft (including substantive translation), Writing – review & editing, Preparation, creation and/or presentation of the published work by those from the original research group, specifically critical review, commentary or revision – including pre-or postpublication stages. **I.M. Ribeiro:** Methodology, Development or design of methodology; creation of models. **T.C.B. Tomassini:** Supervision, Oversight and leadership responsibility for the research activity planning and execution, including mentorship external to the core team. **R.X. Faria:** Conceptualization, Ideas; formulation or evolution of overarching research goals and aims, Methodology, Development or design of methodology; creation of models, Software, Programming, software development; designing computer programs; implementation of the computer code and supporting algorithms; testing of existing code components, Validation – Verification, whether as a part of the activity or separate, of the overall replication/reproducibility of results/experiments and other research outputs, investigation Conducting a research and investigation process, specifically performing the experiments, or data/evidence collection, Writing – original draft, Preparation, creation and/or presentation of the published work, specifically writing the initial draft (including substantive translation), Writing – review & editing, Preparation, creation and/or presentation of the published work by those from the original research group, specifically critical review, commentary or revision – including pre-or postpublication stages, Supervision, Oversight and leadership responsibility for the research activity planning and execution, including mentorship external to the core team, Project administration, Management and coordination responsibility for the research activity planning and execution, Funding acquisition, Acquisition of the financial support for the project leading to this publication.

Author contributions

JCCA, NCR, EGS, LGBF, MLB, CP, TEMMC, JAAS; IMR, TCBT, RXF. Performed the experiments (chemical isolation of the extract, physalin pool, and isolated physalins): IMR and TCBT. Performed the experiments (biological assays): JCCA, NCR, LBGF, TEMMC, JAAS, and RXF. Performed the experiments (in silico assays): EGS, and MLB. Wrote and supervised the paper: RXF, CP, and JAAS.

Conflict of interest statement

The authors declare that they have no known competing financial interests or personal relationships that could have appeared to influence the work reported in this paper.

Appendix A. Supplementary material

Supplementary data associated with this article can be found in the online version at doi:10.1016/j.biopha.2021.112006.

References

[1] R.N. Almeida, R.N. Almeida, D.S. Navarro, J.M. Barbosa-Filho, Plants with central analgesic activity, Phytomedicine 8 (2001) 310–322, https://doi.org/10.1078/0944-7113-00050.

[2] J.S. Silva, M.D. Moura, R.A.G. Oliveira, M.F.F. Diniz, J.M. Barbosa-Filho, Natural product inhibitors of ovarian neoplasia, Phytomedicine 10 (2003) 221–232, https://doi.org/10.1078/094471103321659988.

[3] L.G. Rocha, J.R.G.S. Almeida, R.O. Macêdo, J.M. Barbosa-Filho, A review of natural products with antileishmanial activity, Phytomedicine 12 (2005) 514–535, https://doi.org/10.1016/j.phymed.2003.10.006.

[4] J.M. Barbosa-Filho, F.A. Nascimento Júnior, A.C.A. Tomaz, P.F. Athayde-Filho, M.S. Silva, E.V.L. Cunha, M.F.V. Souza, L.M. Batista, M.F.F.M. Diniz, Natural products with antileprotic activity, Rev. Bras. Farmacogn. 17 (2007) 141–148, https://doi.org/10.1590/S0102-695×2007000100022.

[5] A.C. Siani, B. Gilbert, Riopharma 18, Porto Alegre: UFRGS, 1999, p. 502.

[6] R. Schmid, A.T. Hunziker, Genera Solanacearum: the genera of Solanaceae illustrated, arranged according to a new system, Taxon 50 (2001) 1294, https://doi.org/10.2307/1224768.

[7] K.K. Purushothaman, S. Vasanth, Chemistry and pharmacology of steroids derivatives from Physalis, J. Sci. Ind. Res. (1988). http://www.niscair.res.in/jinfo/JSIR/jsir_inst_auth.pdf.

[8] O.E. Vasina, V.A. Maslennikova, N.K. Abubakirov, Physalis with asteroids, Khim. Priord. Soed. 3 (1986) 243–255.

[9] G.A. Koffuor, P. Amoateng, T.A. Andey, Immunomodulatory and erythropoietic effects of aqueous extract of the fruits of Solanum torvum Swartz (Solanaceae), Pharmacogn. Res. 3 (2011) 130–134, https://doi.org/10.4103/0974-8490.81961.

[10] A.C. Pereira, D.F. Oliveira, G.H. Silva, H.C.P. Figueiredo, A.J. Cavalheiro, D. A. Carvalho, L.P. Souza, S.M. Chalfoun, Identification of the antimicrobial substances produced by Solanum palinacanthum (Solanaceae), An. Acad. Bras. Ciênc. 80 (2008) 427–432, https://doi.org/10.1590/S0001-37652008000300004.

[11] N. Fadl Almoulah, Y. Voynikov, R. Gevrenova, H. Schohn, T. Tzanova, S. Yagi, J. Thomas, B. Mignard, A.A.A. Ahmed, M.A. El Siddig, R. Spina, D. Laurain-Mattar, Antibacterial, antiproliferative and antioxidant activity of leaf extracts of selected Solanaceae species, S. Afr. J. Bot. 112 (2017) 368–374, https://doi.org/10.1016/j.sajb.2017.06.016.

[12] H. Mier-Giraldo, L.E. Díaz-Barrera, L.G. Delgado-Murcia, M.F. Valero-Valdivieso, G. Cáez-Ramírez, Cytotoxic and immunomodulatory potential activity of Physalis peruviana fruit extracts on cervical cancer (HeLa) and fibroblast (L929) cells, J. Evid. Based Complement. Altern. Med. 22 (2017) 777–787, https://doi.org/10.1177/2156587217718751.

[13] J.A.A. Dos Santos, T.C.B. Tomassini, D.C.D. Xavier, I.M. Ribeiro, M.T.G. Da Silva, Z.B. De Morais Filho, Molluscicidal activity of Physalis angulata L. extracts and fractions on Biomphalaria tenagophila (d'Orbigny, 1835) under laboratory conditions, Mem. Inst. Oswaldo Cruz (2003), https://doi.org/10.1590/s0074-02762003000300024.

[14] C.A. Elliger, J.A. Eash, A.C. Waiss, Kaempferol and quercetin di- and triglycosides from Physalis peruviana leaves, Biochem. Syst. Ecol. 20 (1992) 268, https://doi.org/10.1016/0305-1978(92)90063-.

[15] M. Sahai, P. Neogi, Chemical-constituents of Physalins-peruviana roots, J. Ind. Chem. Soc. 61 (1984) 171–172.

[16] T. Chandrasekhara Rao, G. Lakshminarayana, N.B.L. Prasad, S. Jagan Mohan Rao, G. Azeemoddin, D. Atchyuta Ramayya, S.D. Thirumala Rao, Characteristics and compositions of Carissa spinarum, Leucaena leucocephala and physalis minima seeds and oils, J. Am. Oil Chem. Soc. 61 (1984) 1472–1473, https://doi.org/10.1007/BF02636369.

[17] S.K. Mahna, D. Singh, Free ascorbic acid from solanaceous plants and their mutants, Indian J. Pharmacol. (1974).

[18] H. Lorenzi, H.M. de Souza, Plantas ornamentais no Brasil: arbustivas, herbáceas e trepadeiras, Instituto Plantarum de Estudos da Flora, 2001.

[19] Y.S. Lin, H.C. Chiang, W.S. Kan, E. Hone, S.J. Shih, M.H. Won, Immunomodulatory activity of various fractions derived from Physalis angulata L extract, Am. J. Chin. Med. 20 (1992) 233–243, https://doi.org/10.1142/s0192415×92000242.

[20] L. Sun, J. Liu, P. Liu, Y. Yu, L. Ma, L. Hu, The potential role of preventing atherosclerosis by induction of neonatal tolerance to VLDL, Cell. Immunol. 272 (2012) 290–292, https://doi.org/10.1016/j.procbio.2010.09.022.

[21] E.T. Guimarães, M.S. Lima, L.A. Santos, I.M. Ribeiro, T.B.C. Tomassini, R.R. dos Santos, et al., Efeitos de seco-esteróides purificados de Physalis angulata L., Solanaceae na viabilidade de Leishmania sp. Braz. J. Pharmacogn. (2010) https://doi.org/10.1590/S0102-695×2010005000036.

[22] W.-T. Hsieh, K.-Y. Huang, H.-Y. Lin, J.-G. Chung, Physalis angulata induced G2/M phase arrest in human breast cancer cells, Food Chem. Toxicol. 44 (2006) 974–983, https://doi.org/10.1016/j.fct.2005.11.013.

[23] J.K. Hwang, J.S. Shim, J.Y. Chung, Anticariogenic activity of some tropical medicinal plants against Streptococcus mutans, Fitoterapia 75 (2004) 596–598, https://doi.org/10.1016/j.fitote.2004.05.006.

[24] A. Cáceres, H. Menéndez, E. Méndez, E. Cohobón, B.E. Samayoa, E. Jauregui, E. Peralta, G. Carrillo, Antigonorrhoeal activity of plants used in Guatemala for the treatment of sexually transmitted diseases, J. Ethnopharmacol. 48 (1995) 85–88, https://doi.org/10.1016/0378-8741(95)01288-O.

[25] G.N.T. Bastos, A.J.A. Silveira, C.G. Salgado, D.L.W. Picanço-Diniz, J.L.M. do Nascimento, Physalis angulata extract exerts anti-inflammatory effects in rats by inhibiting different pathways, J. Ethnopharmacol. 118 (2008) 246–251, https://doi.org/10.1016/j.jep.2008.04.005.

[26] S.D. Skaper, P. Debetto, P. Giusti, The P2×7 purinergic receptor: from physiology to neurological disorders, FASEB J. 24 (2010) 337–345, https://doi.org/10.1096/fj.09-138883.

[27] S. Roger, P. Pelegrin, P2×7 receptor antagonism in the treatment of cancers, Expert Opin. Investig. Drugs 20 (2011) 875–880, https://doi.org/10.1517/13543784.2011.583918.

[28] M.F. Lister, J. Sharkey, D.A. Sawatzky, J.P. Hodgkiss, D.J. Davidson, A.G. Rossi, K. Finlayson, The role of the purinergic P2×7 receptor in inflammation, J. Inflamm. 4 (2007) 5, https://doi.org/10.1186/1476-9255-4-5.

[29] J.S. Wiley, R. Sluyter, B.J. Gu, L. Stokes, S.J. Fuller, The human P2×7 receptor and its role in innate immunity, Tissue Antigens 78 (2011) 321–332, https://doi.org/10.1111/j.1399-0039.2011.01780.x.

[30] T. Sugiyama, Role of P2×7 receptors in the development of diabetic retinopathy, World J. Diabetes 5 (2) (2014) 141–145, https://doi.org/10.4239/wjd.v5.i2.141.

[31] C.B.M. Platania, F. Lazzara, A. Fidilio, C.G. Fresta, F. Conti, G. Giurdanella, G. M. Leggio, S. Salomone, F. Drago, C. Bucolo, Blood-retinal barrier protection against high glucose damage: the role of P2×7 receptor, Biochem. Pharmacol. 168 (2019) 249–258, https://doi.org/10.1016/j.bcp.2019.07.010.

[32] W. Lu, H. Hu, J. Sévigny, B.T. Gabelt, P.L. Kaufman, E.C. Johnson, J.C. Morrison, G.S. Zode, V.C. Sheffield, X. Zhang, A.M. Laties, C.H. Mitchell, Rat, mouse, and primate models of chronic glaucoma show sustained elevation of extracellular ATP and altered purinergic signaling in the posterior eye, Investig. Ophthalmol. Vis. Sci. 56 (5) (2015) 3075–3083, https://doi.org/10.1167/iovs.14-15891.

[33] Y.M. Wang Anna, H.Y. Wong Vickie, Ying Lee Pei, V. Bui Bang, Kirstan A. Vessey, Stefanie Dudczig, E.L. Fletcher, Retinal ganglion cell dysfunction in mice following acute intraocular pressure is exacerbated by P2×7 receptor knockout, Sci. Rep. 11 (2021) 4184, https://doi.org/10.1038/s41598-021-83669-0.

[34] C.G. Fresta, G. Caruso, D. Fidilio, C.B.M. Platania, N. Musso, F. Caraci, F. Drago, C. Bucolo, Dihydrotanshinone, a natural diterpenoid, preserves blood-retinal barrier integrity via P2×7 receptor, IJMS 21 (23) (2020) 9305, https://doi.org/10.3390/ijms21239305.

[35] G.L. Romano, R. Amato, F. Lazzara, V. Porciatti, T. Chou, F. Drago, C. Bucolo, P2×7 receptor antagonism preserves retinal ganglion cells in glaucomatous mice, Biochem. Pharmacol. 180 (2020), 114199, https://doi.org/10.1016/j.bcp.2020.114199.

[36] C.B.M. Platania, G. Giurdanella, L. Di Paola, F. Drago, S. Salomone, C. Bucolo, P2×7 receptor antagonism: implications in diabetic retinopathy, Biochem. Pharmacol. 138 (15) (2017) 130–139, https://doi.org/10.1016/j.bcp.2017.05.001.

[37] D.C. Broom, D.J. Matson, E. Bradshaw, M.E. Buck, R. Meade, S. Coombs, M. Matchett, K.K. Ford, W. Yu, J. Yuan, S.H. Sun, R. Ochoa, J.E. Krause, D. J. Wustrow, D.N. Cortright, Characterization of N-(adamantan-1-ylmethyl)-5-[(3R-amino-pyrrolidin-1-yl) methyl]-2-chloro-benzamide, a P2×7 antagonist in animal models of pain and inflammation, J. Pharmacol. Exp. Ther. 327 (2008) 620–633, https://doi.org/10.1124/jpet.108.141853.

[38] A.K. Clark, A.A. Staniland, F. Marchand, T.K.Y. Kaan, S.B. McMahon, M. Malcangio, P2×7-dependent release of interleukin-1 and nociception in the spinal cord following lipopolysaccharide, J. Neurosci. 30 (2010) 573–582, https://doi.org/10.1523/JNEUROSCI.3295-09.2010.

[39] A.J. Duplantier, et al., ChemInform abstract: optimization of the physicochemical and pharmacokinetic attributes in a 6-azauracil series of P2×7 receptor antagonists leading to the discovery of the clinical candidate CE-224,535 (I), ChemInform 42 (2011) no, https://doi.org/10.1002/chin.201143159.

[40] N. Arulkumaran, R.J. Unwin, F.W.K. Tam, A potential therapeutic role for P2×7 receptor (P2×7R) antagonists in the treatment of inflammatory diseases, Expert Opin. Investig. Drugs 20 (2011) 897–915, https://doi.org/10.1517/13543784.2011.578068.

[41] A.N. Shemon, R. Sluyter, A.D. Conigrave, J.S. Wiley, Chelerythrine and other benzophenanthridine alkaloids block the human P2×7 receptor, Br. J. Pharmacol. 142 (2004) 1015–1019, https://doi.org/10.1038/sj.bjp.0705868.
[42] M.S. Buchanan, A.R. Carroll, R. Addepalli, V.M. Avery, J.N. Hooper, R.J. Quinn, Natural products, stylissadines A and B, specific antagonists of the P2×7 receptor, an important inflammatory target, J. Org. Chem. 72 (2007) 2309–2317, https://doi.org/10.1021/jo062007q.
[43] J.A.A. Santos, T.C.B. Tomassini, D.C.D. Xavier, I.M. Ribeiro, M.T.G. Silva, Z. B. Morais Filho, Molluscicidal activity of Physalis angulata L. extracts and fractions on Biomphalaria tenagophila (d'Orbigny, 1835) under laboratory conditions, Mem. Inst. Oswaldo Cruz 98 (2003) 425–428, https://doi.org/10.1590/S0074-02762003000300024.
[44] G. Bastos, A. Silveira, C. Salgado, D. Picanco-Diniz, J. Do Nascimento, Physalis angulata extract exerts anti-inflammatory effects in rats by inhibiting different pathways, J. Ethnopharmacol. 118 (2008) 246–251, https://doi.org/10.1016/j.jep.2008.04.005.
[45] M.T.G. Silva, S.M. Simas, T.G. Batista, P. Cardarelli, T.C.B. Tomassini, Studies on antimicrobial activity, in vitro, of Physalis angulata L. (Solanaceae) fraction and physalin B bringing out the importance of assay determination, Mem. Inst. Oswaldo Cruz 100 (2005) 779–782, https://doi.org/10.1590/S0074-02762005000700018.
[46] R.X. Faria, F.H. Oliveira, J.P. Salles, A.S. Oliveira, N.L. von Ranke, M.L. Bello, C. R. Rodrigues, H.C. Castro, A.R. Louvis, D.L. Martins, V.F. Ferreira, 1,4-Naphthoquinones potently inhibiting P2×7 receptor activity, Eur. J. Med. Chem. 143 (2018) 1361–1372, https://doi.org/10.1016/j.ejmech.2017.10.033.
[47] M.S. Lima, A.F. Evangelista, G.G.L. Santos, I.M. Ribeiro, T.C.B. Tomassini, M. B. Pereira Soares, C.F. Villarreal, Antinociceptive properties of physalins from Physalis angulata, J. Nat. Prod. 77 (2014) 2397–2403, https://doi.org/10.1021/np5003093.
[48] R.X. Faria, N. de Jesus Hiller, J.P. Salles, J.A.L.C. Resende, R.T. Diogo, N.L. von Ranke, M.L. Bello, C.R. Rodrigues, H.C. Castro, D. de Luna Martins, Arylboronic acids inhibit P2×7 receptor function and the acute inflammatory response, J. Bioenerg. Biomembr. 51 (2019) 277–290, https://doi.org/10.1007/s10863-019-09802-x.
[49] O. Myhre, J. Andersen, H. Aarnes, F. Fonnum, Evaluation of the probes 20, 70-dichlorofluorescin diacetate, luminol, Biochem. Pharmacol. 65 (10) (2003) 1575–1582, https://doi.org/10.1016/s0006-2952(03)00083-2.
[50] R.X. Faria, F.P. DeFarias, L.A. Alves, Are second messengers crucial for opening the pore associated with P2×7 receptor? Am. J. Physiol. Cell Physiol. 288 (2005) 260–271, https://doi.org/10.1152/ajpcell.00215.2004.
[51] M.D. Hanwell, D.E. Curtis, D.C. Lonie, T. Vandermeerschd, E. Zurek, G. R. Hutchison, Avogadro: an advanced semantic chemical editor, visualization, and analysis platform, J. Cheminform. 4 (2012) 17, https://doi.org/10.1186/1758-2946-4-17.
[52] T.A. Halgren, Merck molecular force field. I. Basis, form, scope, parameterization, and performance of MMFF94, J. Comput. Chem. 17 (1996) 490–519, https://doi.org/10.1002/(SICI)1096-987X(199604)17:5/6<490::AID-JCC1>3.0.CO;2-P.
[53] J.J.P. Stewart, Optimization of parameters for semiempirical methods V: modification of NDDO approximations and application to 70 elements, J. Mol. Model. 13 (2007) 1173–1213, https://doi.org/10.1007/s00894-007-0233-4.
[54] James J.P. Stewart, MOPAC2016, Stewart Computational Chemistry, Color Springs, CO, USA, 2016.
[55] A. Waterhouse, M. Bertoni, S. Bienert, SWISS-MODEL: homology modelling of protein structures and complexes, Nucleic Acids Res. 46 (W1) (2018) W296–W303, https://doi.org/10.1093/nar/gky427.
[56] S. Pundir, M.J. Martin, C. O'Donovan, UniProt protein knowledgebase, in: C. H. Wu, C.N. Arighi, K.E. Ross (Eds.), Protein Bioinformatics: From Protein Modifications and Networks to Proteomics, Springer New York, New York, NY, 2017, pp. 41–55, https://doi.org/10.1007/978-1-4939-6783-4_2.
[57] A. Karasawa, T. Kawate, Structural basis for subtype-specific inhibition of the P2×7 receptor, eLife 5 (2016), https://doi.org/10.7554/eLife.22153.
[58] R.A. Laskowski, M.W. MacArthur, D.S. Moss, J.M. Thornton, PROCHECK: a program to check the stereochemical quality of protein structures, J. Appl. Crystallogr. 26 (1993) 283–291, https://doi.org/10.1107/s0021889892009944.
[59] J. Yang, Y. Zhang, I-TASSER server: new development for protein structure and function predictions, Nucleic Acids Res. 43 (2015) W174–W181, https://doi.org/10.1093/nar/gkv342.
[60] S. Jo, T. Kim, W. Im, Automated builder and database of protein/membrane complexes for molecular dynamics simulations, PLOS One 2 (2007) 880, https://doi.org/10.1371/journal.pone.0000880.
[61] G. Van Meer, D.R. Voelker, G.W. Feigenson, Membrane lipids: where they are and how they behave, Nat. Rev. Mol. Cell Biol. 9 (2008) 112–124, https://doi.org/10.1038/nrm2330.
[62] R. Thomsen, M.H. Christensen, MolDock: a new technique for high-accuracy molecular docking, J. Med. Chem. 49 (2006) 3315–3321, https://doi.org/10.1021/jm051197e.
[63] D. Gonzaga, F.H. Oliveira, N.L. von Ranke, G.Q. Pinho, J.P. Salles, M.L. Bello, C. R. Rodrigues, H.C. Castro, H. de Souza, C. Reis, R. Leme, J. Mafra, L. Pinheiro, L. Hoelz, N. Boechat, R.X. Faria, Synthesis, biological evaluation and molecular modeling studies of new thiadiazole derivatives as potent P2×7 receptor inhibitors, Front. Chem. 7 (2019) 261, https://doi.org/10.3389/fchem.2019.00261.
[64] P.A.F. Pacheco, R.M.S. Galvão, A.F.M. Faria, N. l Von Ranke, M.S. Rangel, T. M. Ribeiro, M.L. Bello, C.R. Rodrigues, V.F. Ferreira, D.R. da Rocha, R.X. Faria, 8-Hydroxy-2-(1H-1,2,3-triazol-1-yl)-1,4-naphtoquinone derivatives inhibited P2×7 receptor-induced dye uptake into murine macrophages, Bioorg. Med. Chem. 27 (2019) 1449–1455, https://doi.org/10.1016/j.bmc.2018.11.036.
[65] M.J. Abraham, T. Murtola, R. Schulz, S. Páll, J.C. Smith, B. Hess, E. Lindahl, Gromacs: high performance molecular simulations through multi-level parallelism from laptops to supercomputers, SoftwareX 1–2 (2015) 19–25, https://doi.org/10.1016/j.softx.2015.06.001.
[66] E.F. Pettersen, T.D. Goddard, C.C. Huang, G.S. Couch, D.M. Greenblatt, E. C. Meng, T.E. Ferrin, UCSF Chimera – a visualization system for exploratory research and analysis, J. Comput. Chem. 25 (2004) 1605–1612, https://doi.org/10.1002/jcc.20084.
[67] J. Lee, X. Cheng, J.M. Swails, M.S. Yeom, P.K. Eastman, J.A. Lemkul, S. Wei, J. Buckner, J.C. Jeong, Y. Qi, S. Jo, V.S. Pande, D.A. Case, C.L. Brooks, A. D. MacKerell, J.B. Klauda, W. Im, CHARMM-GUI input generator for NAMD, GROMACS, AMBER, OpenMM, and CHARMM/openMM simulations using the CHARMM36 additive force field, J. Chem. Theory Comput. 12 (2016) 405–413, https://doi.org/10.1021/acs.jctc.5b00935.
[68] W. Yu, X. He, K. Vanommeslaeghe, A.D. MacKerell, Extension of the CHARMM general force field to sulfonyl-containing compounds and its utility in biomolecular simulations, J. Comput. Chem. 33 (2012) 2451–2468, https://doi.org/10.1002/jcc.23067.
[69] B. Hess, C. Kutzner, D. Van Der Spoel, E. Lindahl, GROMACS 4: algorithms for highly efficient, load-balanced, and scalable molecular simulation, J. Chem. Theory Comput. 4 (2008) 435–447, https://doi.org/10.1021/ct700301q.
[70] U. Essmann, L. Perera, M.L. Berkowitz, T. Darden, H. Lee, L.G. Pedersen, A smooth particle mesh Ewald method, J. Chem. Phys. 103 (1995) 8577–8593, https://doi.org/10.1063/1.470117.
[71] G. Bussi, D. Donadio, M. Parrinello, Canonical sampling through velocity rescaling, J. Chem. Phys. 126 (2007), 014101, https://doi.org/10.1063/1.2408420.
[72] S.M. Rogge, L. Vanduyfhuys, A. Ghysels, M. Waroquier, T. Verstraelen, G. Maurin, V. Van Speybroeck, A comparison of barostats for the mechanical characterization of metal-organic frameworks, J. Chem. Theory Comput. 11 (2015) 5583–5597, https://doi.org/10.1021/acs.jctc.5b00748.
[73] M. Parrinello, A. Rahman, Polymorphic transitions in single crystals: a new molecular dynamics method, J. Appl. Phys. 52 (1981) 7182–7190, https://doi.org/10.1063/1.328693.
[74] R. Kumari, R. Kumar, A. Lynn, g_mmpbsa–a GROMACS tool for high-throughput MM-PBSA calculations, J. Chem. Inf. Model. 54 (2014) 1951–1962, https://doi.org/10.1021/ci500020m.
[75] M. Huang, J. He, H. Hu, K. Zhang, X. Wang, B. Zhao, H. Lou, D. Ren, T. Shen, Withanolides from the genus physalis: a review on their phytochemical and pharmacological aspects, J. Pharm. Pharmacol. 72 (2020) 649–669, https://doi.org/10.1111/jphp.13209.
[76] R.F. Espírito Santo, M.S. Lima, P.J.L. Juiz, L.C.F. Opretzka, R.C. Nogueira, I. M. Ribeiro, T.C.B. Tomassini, M.B.L. Soares, C.F. Villarreal, Physalis angulata concentrated ethanolic extract suppresses nociception and inflammation by modulating cytokines and prostanoids pathways, Nat. Prod. Res. (2019) 1–5, https://doi.org/10.1080/14786419.2019.1705812.
[77] R.C. Nogueira, V.P. Rocha, F.R. Nonato, T.C. Tomassini, I.M. Ribeiro, R.R. dos Santos, B. Soares, Genotoxicity and antileishmanial activity evaluation of Physalis angulata concentrated ethanolic extract, Environ. Toxicol. Pharmacol. 36 (2013) 1304–1311, https://doi.org/10.1016/j.etap.2013.10.013.
[78] R. Coutinho-Silva, D.M. Ojcius, D.C. Górecki, P.M. Persechini, R.C. Bisaggio, A. N. Mendes, J. Marks, G. Burnstock, P.M. Dunn, Multiple P2X and P2Y receptor subtypes in mouse J774, spleen and peritoneal macrophages, Biochem. Pharmacol. 69 (2005) 641–655, https://doi.org/10.1016/j.bcp.2004.11.012.
[79] A.H. Januário, E.R. Filho, R.C.L.R. Pietro, S. Kashima, D.N. Sato, S.C. França, Antimycobacterial physalins from Physalis angulata L. (Solanaceae), Phytother. Res. 16 (2002) 445–448, https://doi.org/10.1002/ptr.939.
[80] R.X. Faria, C.M. Cascabulho, R.A. Reis, L.A. Alves, Large-conductance channel formation mediated by P2×7 receptor activation is regulated through distinct intracellular signaling pathways in peritoneal macrophages and 2BH4 cells, Naunyn Schmiedebergs Arch. Pharmacol. 382 (2010) 73–87, https://doi.org/10.1007/s00210-010-0523-8.
[81] M.B.P. Soares, D. Brustolim, L.A. Santos, M.C. Bellintani, F.P. Paiva, Y.M. Ribeiro, Physalins B, F and G, seco-steroids purified from Physalis angulata L., inhibit lymphocyte function and allogeneic transplant rejection, Int. Immunopharmacol. 6 (2006) 408–414, https://doi.org/10.1016/j.intimp.2005.09.007.
[82] D.J.F. Brustolim, V.L.A.R. Freitas, M.M. Teixeira, M.T. Farias, Y.M. Ribeiro, T.C. B. Tomassini, G.G.S. Oliveira, L.C. Pontes-de-Carvalho, R. Ribeiro-dos-Santos, M. B.P. Soares, Activity of physalin F in a collagen-induced arthritis model, J. Nat. Prod. 73 (2010) 1323–1326.
[83] K.R. Rathore, S.S. Dutt, D. Lokesh, Antiasthmatic activity of the methanolic extract of Physalis angulata Linn, J. Med. Plants Res. 5 (5351–5355) (2011) 16.
[84] M.B.P. Soares, M.C. Bellintani, I.M. Ribeiro, T.C.B. Tomassini, R.R. Santos, Inhibition of macrophage activation and lipopolysaccaride-induced death by seco-steroids purified from Physalis angulata L, Eur. J. Pharmacol. 459 (2003) 107–112, https://doi.org/10.1016/s0014-2999(02)02829-7.
[85] J. Park, J. Kim, P2×7 receptor antagonists: a patent review (2010–2015), Expert Opin. Ther. Pat. 27 (2017) 257–267, https://doi.org/10.1080/13543776.2017.1246538.
[86] J. Villar, A.S. Slutsky, GOLDEN anniversary of the acute respiratory distress syndrome: still much work to do!, Curr. Opin. Crit. Care 23 (2017) 4–9, https://doi.org/10.1097/MCC.0000000000000378.
[87] C. Mason, N. Dooley, M. Griffiths, Acute respiratory distress syndrome, Clin. Med. 16 (2016) s66–s70, https://doi.org/10.7861/clinmedicine.16-6-s66.

[88] R.C. Nogueira, V.P. Rocha, F.R. Nonato, T.C. Tomassini, I.M. Ribeiro, R.R. dos Santos, B. Soares, Genotoxicity and antileishmanial activity evaluation of Physalis angulata concentrated ethanolic extract, Environ. Toxicol. Pharmacol. 36 (2013) 1304–1311, https://doi.org/10.1016/j.etap.2013.10.013.
[89] R.J. Soares-Bezerra, N.C. Silva Ferreira, T.M. Almeida Alves, C.L. Zani, L.H. Rosa, R.X. Faria, V. Silva Frutuoso, L.A. Alves, A new insight into purinergic pharmacology: three fungal species as natural P2×7R antagonists, Phytother. Res. 33 (2019) 2319–2328, https://doi.org/10.1002/ptr.6412.
[90] J.A.A. Santos, A.A. Fidalgo-Neto, R.X. Faria, A. Simões, A.S. Calheiros, A. L. Bérenger, H.C.C. Faria-Neto, M.R. Figueiredo, V.S.L. Frutuoso, L.A. Alves, Effect of rheedia longifolia leaf extract and fractions on the P2×7 receptor in vitro: novel antagonists? J. Med. Food 14 (2011) 920–929, https://doi.org/10.1089/jmf.2010.0184.
[91] C. Rathore, K.R. Dutt, S. Sahu, L. Deb, Antiasthmatic activity of the methanolic extract of Physalis angulata linn, J. Med. Plant Res. (2011), https://doi.org/10.5897/JMPR.9000118.
[92] G.N. Bastos, A.R. Santos, V.M. Ferreira, A.M. Costa, C.I. Bispo, A.J. Silveira, J. L. Do Nascimento, Antinociceptive effect of the aqueous extract obtained from roots of Physalis angulata L. on mice, J. Ethnopharmacol. 103 (2006) 241–245, https://doi.org/10.1016/j.jep.2005.08.008.
[93] D.T.G Gonzaga, L.B.G Ferreira, T.E. Moreira Maramaldo Costa, N.L. von Ranke, P. Anastácio Furtado Pacheco, AP Sposito Simões, et al., 1-Aryl-1H- and 2-Aryl-2H-1,2,3-Triazole Derivatives Blockade P2×7.
[94] F. Hu, F. Xing, G. Zhu, G. Xu, C. Li, J. Qu, I. Lee, L. Pan, Rhein antagonizes P2×7 receptor in rat peritoneal macrophages, Sci. Rep. 5 (2015) 14012, https://doi.org/10.1038/srep14012.
[95] C. Marques-Da-Silva, M.M. Chaves, N.G. Castro, R. Coutinho-Silva, M.Z. P. Guimaraes, Colchicine inhibits cationic dye uptake induced by ATP in P2×2 and P2×7 receptor-expressing cells: implications for its therapeutic action, Br. J. Pharmacol. 163 (2011) 912–926, https://doi.org/10.1111/j.1476-5381.2011.01254.x.
[96] W. Fischer, N. Urban, K. Immig, H. Franke, M. Schaefer, Natural compounds with P2×7 receptor-modulating properties, Purinergic Signal. 10 (2014) 313–326, https://doi.org/10.1007/s11302-013-9392-1.
[97] F. Hu, F. Xing, G. Zhu, G. Xu, C. Li, J. Qu, I. Lee, L. Pan, Rhein antagonizes P2×7 receptor in rat peritoneal macrophages, Sci. Rep. 5 (2015) 14012, https://doi.org/10.1038/srep14012.
[98] L. Liu, J. Zou, X. Liu, L.H. Jiang, J. Li, Inhibition of ATP-induced macrophage death by emodin via antagonizing P2×7 receptor, Eur. J. Pharmacol. (2010), https://doi.org/10.1016/j.ejphar.2010.04.036.
[99] S. Zhu, Y. Wang, X. Wang, J. Li, F. Hu, Emodin inhibits ATP-induced IL-1β secretion, ROS production and phagocytosis attenuation in rat peritoneal macrophages via antagonizing P2×7 receptor, Pharm. Biol. 52 (2014) 51–57, https://doi.org/10.3109/13880209.2013.810648.
[100] D.T.G. Gonzaga, F.H. Oliveira, N.L. von Ranke, G.Q. Pinho, J.P. Salles, M.L. Bello, C.R. Rodrigues, H.C. Castro, H.V.C.M. de Souza, C.R.C. Reis, R.P.P. Leme, J.C. M. Mafra, L.C.S. Pinheiro, L.V.B. Hoelz, N. Boechat, R.X. Faria, Synthesis, biological evaluation, and molecular modeling studies of new thiadiazole derivatives as potent P2×7 receptor inhibitors, Front. Chem. 7 (2019) 261, https://doi.org/10.3389/fchem.2019.00261.
[101] M. Da Silva Lima, A.F. Evangelista, G.G.L. Dos Santos, I.M. Ribeiro, T.C. B. Tomassini, M.B. Pereira Soares, et al., Antinociceptive properties of physalins from Physalis angulata, J. Nat. Prod. (2014), https://doi.org/10.1021/np5003093.
[102] K.-Y. Yang, M.-D. Kim, J.-S. Ju, M.-J. Kim, D.-K. Ahn, Participation of central P2×7 receptors in CFA-induced inflammatory pain in the orofacial area of rats, Int. J. Oral Biol. 39 (2014) 49–56, https://doi.org/10.11620/ijob.2014.39.1.049.
[103] T.R. Martin, Neutrophils and lung injury: getting it right, J. Clin. Investig. 110 (2002) 1603–1605, https://doi.org/10.1172/JCI0217302.
[104] D. Shah, F. Romero, W. Stafstrom, M. Duong, R. Summer, Extracellular ATP mediates the late phase of neutrophil recruitment to the lung in murine models of acute lung injury, Am. J. Physiol. Lung Cell. Mol. Physiol. 306 (2014) 152–161, https://doi.org/10.1152/ajplung.00229.2013.
[105] L.C. Monção-Ribeiro, D.S. Faffe, P.T. Santana, F.S. Vieira, C.L.A.L. Graça, C. Marques-da-Silva, M.N. Machado, C. Caruso-Neves, W.A. Zin, R. Borojevic, C. M. Takiya, R. Coutinho-Silva, P2×7 receptor modulates inflammatory and functional pulmonary changes induced by silica, PLOS One 9 (2014), 110185, https://doi.org/10.1371/journal.pone.0110185.
[106] H. Matsuyama, F. Amaya, S. Hashimoto, H. Ueno, S. Beppu, M. Mizuta, N. Shime, A. Ishizaka, S. Hashimoto, Acute lung inflammation and ventilator-induced lung injury caused by ATP via the P2Y receptors: an experimental study, Respir. Res. 9 (2008) 79, https://doi.org/10.1186/1465-9921-9-79.
[107] Q. Zhang, X. Tao, S. Xia, J. Qu, H. Song, J. Liu, et al., Emodin attenuated severe acute pancreatitis via the P2X ligand-gated ion channel 7/NOD-like receptor protein 3 signaling pathway, Oncol. Rep. (2019), https://doi.org/10.3892/or.2018.6844.
[108] H. Chen, C. Bai, X. Wang, The value of the lipopolysaccharide-induced acute lung injury model in respiratory medicine, Expert Rev. Respir. Med. 4 (2010) 773–783, https://doi.org/10.1586/ers.10.71.
[109] S. Cicko, M. Lucattelli, T. Müller, M. Lommatzsch, G. De Cunto, S. Cardini, Purinergic receptor inhibition prevents the development of smoke-induced lung injury and emphysema, J. Immunol. 185 (2010) 688–697, https://doi.org/10.4049/jimmunol.0904042.
[110] R. Fusco, E. Gugliandolo, F. Biundo, M. Campolo, R. Di Paola, S. Cuzzocrea, Inhibition of inflammasome activation improves lung acute injury induced by carrageenan in a mouse model of pleurisy, FASEB J. 31 (2017) 3497–3511, https://doi.org/10.1096/fj.201601349R.
[111] D. Brustolim, J.F. Vasconcelos, L.A. Freitas, M.M. Teixeira, M.T. Farias, Y. M. Ribeiro, T.C. Tomassini, G.G. Oliveira, L.C. Pontes-de-Carvalho, R. Ribeiro-dos-Santos, M.B. Soares, Activity of physalin F in a collagen-induced arthritis model, J. Nat. Prod. 73 (2010) 1323–1326, https://doi.org/10.1021/np900691w.
[112] N. Ding, Y. Wang, C. Dou, F. Liu, G. Guan, K. Wei, J. Yang, M. Yang, J. Tan, W. Zeng, C. Zhu, Physalin D regulates macrophage M1/M2 polarization via the STAT1/6 pathway, J. Cell Physiol. 234 (2019) 8788–8796, https://doi.org/10.1002/jcp.27537.
[113] Z. Chen, N. Jin, T. Narasaraju, J. Chen, L.R. McFarland, M. Scott, et al., Identification of two novel markers for alveolar epithelial type I and II cells, Biochem. Biophys. Res. Commun. (2004), https://doi.org/10.1016/j.bbrc.2004.05.048.
[114] Y. Guo, A. Mishra, T. Weng, N.R. Chintagari, Y. Wang, C. Zhao, C. Huang, L. Liu, Wnt3a mitigates acute lung injury by reducing P2×7 receptor-mediated alveolar epithelial type i cell death, Cell Death Dis. 5 (2014), e1286, https://doi.org/10.1038/cddis.2014.254.
[115] P.S. Tang, M. Mura, R. Seth, M. Liu, Acute lung injury and cell death: how many ways can cells die? Am. J. Physiol. Lung Cell. Mol. Physiol. 294 (2008) 632–641, https://doi.org/10.1152/ajplung.00262.2007.
[116] K.H. Albertine, M.F. Soulier, Z. Wang, A. Ishizaka, S. Hashimoto, G. A. Zimmerman, M.A. Matthay, L.B. Ware, Fas and Fas ligand are up-regulated in pulmonary edema fluid and lung tissue of patients with acute lung injury and the acute respiratory distress syndrome, Am. J. Pathol. 161 (2002) 1783–1796, https://doi.org/10.1016/S0002-9440(10)64455-0.
[117] S. Herold, W. von Wulffen, M. Steinmueller, S. Pleschka, W.A. Kuziel, M. Mack, M. Srivastava, W. Seeger, U.A. Maus, J. Lohmeyer, Alveolar epithelial cells direct monocyte transepithelial migration upon influenza virus infection: impact of chemokines and adhesion molecules, J. Immunol. 177 (2006) 1817–1824, https://doi.org/10.4049/jimmunol.177.3.1817.
[118] X. Ma, D. Xu, Y. Ai, G. Ming, S. Zhao, Fas inhibition attenuates lipopolysaccharide-induced apoptosis and cytokine release of rat type II alveolar epithelial cells, Mol. Biol. Rep. 37 (2010) 3051–3056, https://doi.org/10.1007/s11033-009-9876-9.
[119] D. Urich, J.L. Eisenberg, K.J. Hamill, D. Takawira, S.E. Chiarella, S. Soberanes, A. Gonzalez, F. Koentgen, T. Manghi, S.B. Hopkinson, A.V. Misharin, H. Perlman, G.M. Mutlu, G.R. Budinger, J.C. Jones, Lung-specific loss of the laminin α3 subunit confers resistance to mechanical injury, J. Cell Sci. 124 (2011) 2927–2937, https://doi.org/10.1164/rccm.201002-0181OC.